Solar Energy 209 (2020) 515–537

Contents lists available at ScienceDirect

Solar Energy

journal homepage: www.elsevier.com/locate/solener

A review on atomic layer deposited buffer layers for Cu(In,Ga)Se_2 (CIGS) thin film solar cells: Past, present, and future

Soumyadeep Sinha [a,1,*], Dip K. Nandi [b,1], Pravin S. Pawar [c,1], Soo-Hyun Kim [b,*], Jaeyeong Heo [c,*]

[a] Department of Physics, Madanapalle Institute of Technology & Science, Madanapalle 517325, Andhra Pradesh, India
[b] School of Materials Science and Engineering, Yeungnam University, 214-1, Dae-dong, Gyeongsan-si 38541, Republic of Korea
[c] Department of Materials Science and Engineering, and Optoelectronics Convergence Research Center, Chonnam National University, Gwangju 61186, Republic of Korea

ARTICLE INFO

Keywords:
Atomic layer deposition
Thin film solar cell
Buffer layer
Cu(In,Ga)Se_2
Power conversion efficiency

ABSTRACT

CIGS-based thin film solar cell (TFSC) technology is emerging as a promising contributor to the solar photovoltaic industry next to the presently leading Si-based technology. Although the theoretical limit of power conversion efficiency (*PCE*) is as high as 33.5%, the highest experimental *PCE* so far just exceeded 20% in the past several years. Therefore, significant efforts are still continuing for further performance enhancement of these cells. Considering that the buffer layer has been identified as one of the key factors, the efforts to replace state-of-the-art but toxic CdS buffer layer have yielded promising results. Several studies showed that the alternative buffer layers grown with environmentally benign materials could even produce a better performance than the CdS-based TFSCs. In this regard, atomic layer deposition (ALD) has been proved as one of the best techniques for depositing the alternative buffer layers. Several Zn-based ternary and few other binary (*e.g.* In_2S_3) compounds have been investigated to realize an optimum ALD-grown buffer layer. In the recent year, a record *PCE* of 23.35% was achieved using ALD-grown ZnMgO buffer layer along with chemical bath deposited Zn(O,S,OH) for CIGSSe TFSC. However, in general the ALD-grown buffer layers only could provide *PCEs* well below 20%. The article presents a comprehensive survey on rapid increase in *PCE* for several ALD-grown buffer layers during the early period followed by a trend of saturation. Finally, the article discusses the current challenges and future scopes/possibilities for the ALD-grown buffer layers as potential alternatives of CdS toward practical applications of CIGS TFSC.

1. Introduction

The first study on a solar cell with ternary chalcopyrite-type absorber ($CuInSe_2$) was performed in the early fifties, followed by improvements and modifications on a continuous basis mainly under the name of CIGS [Cu(In,Ga)Se_2] thin-film solar cells (TFSCs). The recent market share of CIGS-based solar panels is ~2% of total PV production which is next to the CdTe-based panels (~5%) (Ramanujam and Singh, 2017). However, the Si-based solar PV retains the largest market share (~92%) (Ramanujam and Singh, 2017). While Si-based PV technology is energy intensive and expensive and CdTe technology has issues related to toxicity, CIGS technology is free of these issues. In addition, CIGS is easier to synthesize compared to the complex Si wafer fabrication, and therefore its pay-back period is short. These advantages helped CIGS technology attract considerable research and a number of technology transfers, resulting in commercial production lines that collectively reduced the cost over the past few years (CIGS-PV, 2015, 2019).

A typical CIGS-based TFSC is basically a heterojunction solar cell that consists of a conventional film stack such as soda lime glass (SLG)/Mo/CIGS/buffer layer/window layer with a metal contact (Fig. 2a). Here the CIGS absorber and buffer layer are two different types of materials with different bandgaps and/or band edge positions that forms the *p-n* junction in the TFSCs. Like any other solar cells, the formation of this *p-n* junction is also crucial in TFSCs to obtain high device efficiency. Therefore, the optical, electrical, and chemical properties of both of these layers (CIGS and buffer) directly influence the performance of the devices. Buffer layers are mostly *n-type* materials with a higher bandgap (low optical absorption) in comparison to the absorber materials that allows the light reaching the absorber layer. These layers are with an optimal rage of 50–80-nm-thick to retain minimal series resistance. Moreover, a buffer layer should result in an improved band alignment

* Corresponding authors.
E-mail addresses: drsoumyadeepsinha@mits.ac.in (S. Sinha), soohyun@ynu.ac.kr (S.-H. Kim), jheo@jnu.ac.kr (J. Heo).
[1] These authors contributed equally.

https://doi.org/10.1016/j.solener.2020.09.022
Received 18 June 2020; Received in revised form 28 August 2020; Accepted 9 September 2020
Available online 24 September 2020

Nomenclature

S	area of a cell
E_c	conduction band minimum
ΔE_c	conduction band offset
E_g	optical energy bandgap (or bandgap)
E_f	fermi level
E_v	valence band maximum
J-V	current density–voltage
J-V-T	temperature dependent current density–voltage
J_{sc} *(or* I_{sc}*)*	short circuit current density (or current)
η/ζ	power conversion efficiency
J_0	reverse saturation current
R_p *(or* R_{sh}*)*	parallel (or shunt) resistance
R_s	series resistance
ρ	resistivity
d	buffer layer thickness
T_{sub}/T_{dep}	deposition temperature
V_{oc}	open circuit voltage
n	diode ideality factor
λ	wavelength

Abbreviations

ALCVD	Atomic layer chemical vapor deposition
ALD	Atomic layer deposition
ALE	Atomic layer epitaxy
AR	Anti-reflection
CBD	Chemical bath deposition
CBO	Conduction band offset
CBM	Conduction band minimum
CdTe	Cadmium telluride
CIGS	Copper indium gallium diselenide [$Cu(In,Ga)Se_2$]
CIGSSe	Copper indium gallium disulfoselenide [$Cu(In,Ga)(S,Se)_2$]
CIS	Copper indium disulfide [$CuInS_2$]
CVD	Chemical vapor deposition
CZTS	Copper zinc tin sulfide [Cu_2ZnSnS_4]
CZTSSe	Copper zinc tin sulfur-selenium [$Cu_2ZnSn(S,Se)_4$]
DEZ	Diethylzinc
DB	Dichlorobenzene
EQE	External quantum efficiency
FF	Fill factor
HLS	Heat-light soaking
IC	Integrated circuit
i-ZnO	Intrinsic zinc oxide
MBE	Molecular beam epitaxy
MOCVD	Metal organic chemical vapor deposition
PCE	Power conversion efficiency
PV	Photovoltaic
PDT	Post-deposition treatment
PPC	Persistent photoconductivity
PVD	Physical vapor deposition
RT	Room temperature
S-ALD	Spatial atomic layer deposition
SAS	Selenization and sulfurization
SLG	Soda lime glass
TCO	Transparent conducting oxide
TFSC	Thin film solar cell
VBM	Valence band maximum

between the absorber and window layer that increases the depletion layer, which leads to an enhanced open circuit voltage (V_{oc}) and power conversion efficiency (*PCE*) of the device. In addition to the high optical throughput, a heterojunction with two different semiconductor-based devices is also advantageous to reduce the recombination phenomenon in the wide bandgap buffer layer via efficient charge separation and transport between the absorber and the window layer as compared to that in homojunctions. However, for the heterojunctions, the interface recombination probability is more owing to the presence of defect states at the junction, which can be reduced with the help of a buffer layer and other window layers optimization by realizing favorable band-bending. In addition, a proper formation of conduction band offset (CBO) at the absorber/buffer layer interface is also one of the most essential factors in order to accomplish a high device performance. In an ideal solar cell, the photo-generated electrons-holes are separated by permitting through only one type of charge carriers with the proper distribution of energy band discontinuity at the absorber/buffer interface. In such a consequence, while a large barrier exists for the majority carriers, there will be no band offset for the minority carriers. Furthermore, a buffer layer also helps both in protection of the absorber from damage during the sputter deposition of the oxide window layers as well as passivates large area devices in the production scale (Bakke et al., 2011).

With a rigorous research on *p-type* CIGS absorber material and state-of-the-art chemical bath deposited (CBD) *n-type* CdS buffer layer, the *PCE* of these TFSCs reached above 20% progressively over the past few years (Green et al., 2017, 2018; Jackson et al., 2016; Menner et al., 2017). Moreover, the *PCE* exceeds 20% in the case of the CIGS TFSCs fabricated on flexible substrates which may find potential applications in building-integrated photovoltaics (Chirilă et al., 2013). Nevertheless, on a module scale, CIGS still lags behind Si considerably, the respective average *PCEs* being 16% and 25% (Lee and Ebong, 2017). Nonetheless, there is ample scope to increase the *PCE* of CIGS technology as discussed in this current article. The state-of-the-art CBD-CdS buffer layer has been used in CIGS-based TFSCs successfully for several years since the time it was established. However, more recently, it is being replaced because of its disadvantages such as environmental hazardousness and significant loss of photo-current generated in the buffer and window layers. It is the bandgap of 2.4 eV of CdS that causes the loss in photo-current corresponding to a wavelength region of 350–500 nm. Moreover, the wet-chemical synthesis of CdS often encounters severe incompatibility with rest of the vacuum-based process used to fabricate CIGS TFSCs. All of these disadvantages were the driving factors to explore an alternative material for CdS, and primarily Zn or In-based compounds were found to be one of the most suitable materials for this purpose. Among several materials based on these two elements, ZnO and In_2S_3 find highest number of attempts as binary compounds in this regard. Here, one should also note that these two materials are also successfully tried to form a *p-n* junction by depositing several methods (such as CBD, CVD, sol–gel, sputtering, spray pyrolysis, ALD *etc*.) in other types of TFSCs (like Cu_2O, Sb_2Se_3, CZTS, CZTSSe-based *etc*.) or in perovskite solar cell (Campbell et al., 2020; Kim et al., 2020; Mughal et al., 2015; Platzer-Björkman et al., 2019; Sáez-Araoz et al., 2012; Siol et al., 2016; Tran et al., 2018; Wang et al., 2020, 2017; Wen et al., 2017; Yang et al., 2019; Zang, 2018). However, as far CIGS TFSC is concerned, CBD-grown ZnS(O,OH) or atomic layer deposited (ALD) Zn(O,S) were identified as the best replacement materials among others (Naghavi et al., 2010). ALD contributed significantly towards establishing alternative Cd-free buffer layers over the decades.

ALD, one of the most precise thin film deposition technologies, differs from other similar technologies by the sequential dosing of the reactants commonly known as the precursors that lead to a surface-limited reaction (by chemisorption) with the surface species on the substrate. Thus, ALD results in self-limiting growth and offers a uniform and conformal film over a large surface area and even with a very high aspect

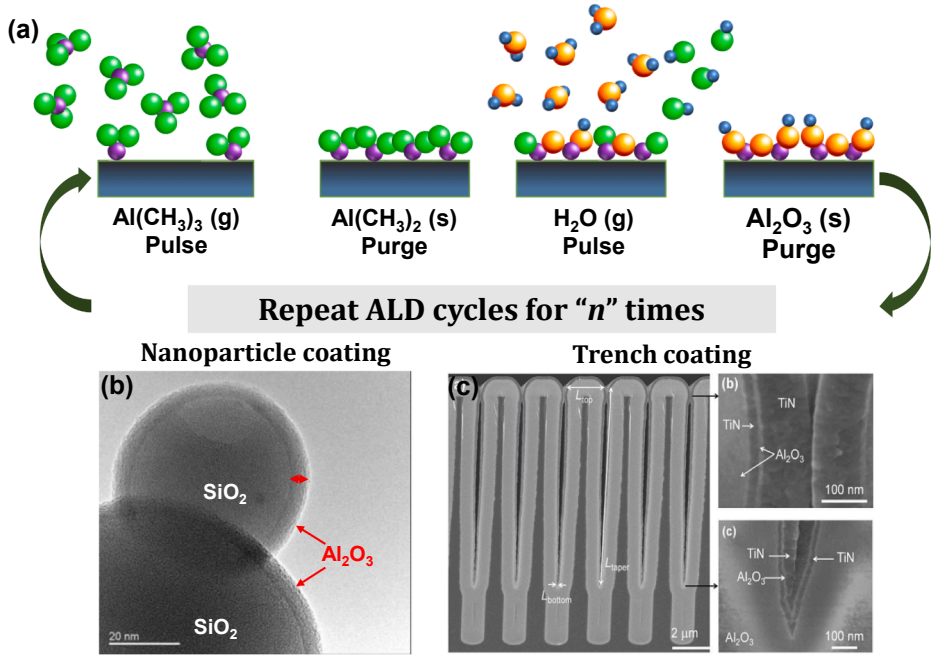

Fig. 1. (a) Schematic representation of an ALD cycle (Al_2O_3) with the sequential exposure of the ALD precursors [Trimethylaluminium ($Al(CH_3)_3$) and H_2O]. ALD-grown films on complex 3D structures like (b) nanoparticles and (c) trench with high aspect ratio. [Reprinted with permission from Hakim et al. (Hakim et al., 2005) and Burke et al. (Burke et al., 2015) Copyright 2005 and 2015, John Wiley and Sons and American Vacuum Society].

ratio. The thickness can be controlled up to angstrom (Å) level with high precision of this technology. Fig. 1 shows a representative ALD cycle along with the ALD-grown films on complex 3-dimentional (3D) structures like nanoparticles or a trench with high aspect ratio. Over time, ALD has found applications in renewable energy that includes solar PV, secondary batteries (*e.g.* Li-ion or Na-ion batteries), supercapacitors, and solar water splitting (Dhara et al., 2020; Guan and Wang, 2016; Li et al., 2018; Nandi et al., 2018, 2019; O'Neill et al., 2015; Ramesh et al., 2020; Sinha et al., 2018a, 2018b, 2019a, 2019b; Wang et al., 2014; Delft et al., 2012). Therefore, this technology can now be considered as a successful tool that reaches far beyond the semiconductor IC industries. In solar PV, fabrication of a buffer layer especially for a CIGS-based TFSC is a major application of ALD.

A wide variety alternative buffer layers in TFSCs are possible to deposit by ALD. As the ALD takes place via chemisorption reaction with the surface species in a self-limiting nature, thus it is capable, in principle, to provide a best possible interface at CIGS/buffer layer junction, which would have low interface defects and thereby, associated recombination. Moreover, ALD enables us to tune the opto-electronic properties of a buffer layer by controlling the stoichiometry of the material especially for a ternary buffer layer. Therefore, a desired band offset can easily be achieved by varying the elemental composition with a precise control of delivering the precursors during film's growth. Last but not the least, it is already mentioned that the minimum adjustable thickness (growth per ALD cycle) by this technique would be in angstrom level (~1–2 Å if not less) which further provides a scope for easy optimization of the buffer layer thickness to a highest precision level if/when necessary. Thus, ALD should be regarded as a superior technique in view of a buffer layer deposition when compared to other wet-chemical or gas-phase film synthesis techniques, in addition to an added advantage of the reduction in the risk of surface damage to the absorber layer by any physical vapor deposition (PVD; like sputtering) techniques.

In this review article, we present a study on ALD-grown buffer layers used in CIGS-based TFSCs till date in a detailed and chronological manner. The article first sets the necessary background needed for it in the introductory section. The central part of the article discusses the findings on different ALD-grown buffer layers used in CIGS-based TFSCs. The article also brings out the current challenges associated with this field and the possible future scopes for the same.

2. Atomic layer deposition in thin film solar cells

As mentioned in the previous section, ALD has already been established as an effective tool in several fields of energy applications. Solar PV is one of the most popular renewable energy fields where ALD has been implemented since the early 1990s. In 1994, Hayafuji et al. reported the application of ALD, which was then known as atomic layer epitaxy (ALE), in an AlGaAs/GaAs multijunction solar cell for the first time (Hayafuji et al., 1994). Similarly, an $Al_{0.3}Ga_{0.7}As$/GaAs based tandem solar cell was also developed by using the ALE (Eldallal et al., 1995). In 1995, the ALD was reported to grow ZnSe buffer layer for a CIGS TFSC (Ohtake et al., 1995). After a few years, ALD was used to deposit B-doped ZnO films as the transparent conducting oxide (TCO) layer of an amorphous Si solar cell (Baosheng et al., 1998, 1999). However, during the past few years, there has been a significant increase in the application of ALD in several fields of solar PV that includes a very effective approach to achieve absorber layer, an ultrathin surface passivation layer, an *n-type* buffer (<100 nm), a transparent front contact and a window layer for different TFSCs (Bakke et al., 2011; Delft et al., 2012; Sinha et al., 2018a). Recently, ALD has mostly been used to deposit surface passivation layers or diffusion barrier layers at the back contact/absorber or absorber/buffer interface to reduce the carrier recombination. The various physical and chemical phenomena at these interfaces cause unfavorable band alignment and interfacial states, increasing the carrier recombination and thereby reducing the device *PCE* (Kaur et al., 2017). The ALD helps to optimize the band alignment using a wide bandgap material (*e.g.* Al_2O_3) that reduces interfacial recombination by reacting with surface defects. In addition, hydrogen sources including precursors and reactants induce the chemical passivation (Kotipalli et al., 2015; Park et al., 2018; Vermang et al., 2014, 2013; Wang et al., 2015; Wu et al., 2014). However, the ALD produces uniform Cd-free binary or ternary metal oxides or sulfides as buffer

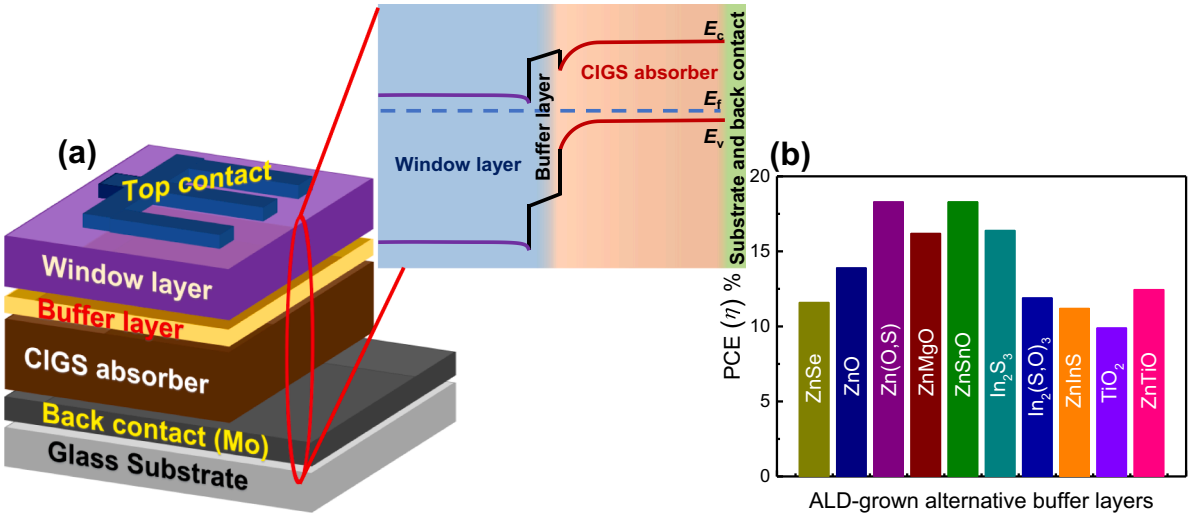

Fig. 2. (a) Basic structure of a typical CIGS-based TFSC (Inset shows a schematic of the band diagram of CIGS-based TFSC) and (b) Graphical representation of the highest *PCE*s achieved for CIGS-based TFSCs with different ALD-grown buffer layers till date (Bugot et al., 2018; Chaisitsak et al., 2000; Genevée et al., 2015; Hsu et al., 2015; Hwang et al., 2018; Kobayashi et al., 2013; Lindahl et al., 2016; Naghavi et al., 2003; Ohtake et al., 1995; Platzer-Björkman et al., 2007).

layers with low defect density in TFSCs at a relatively low growth temperature (Kan et al., 2018). Furthermore, ALD controls the composition of a thin film, especially for a ternary material, by varying the precursor pulse ratios during the deposition, thereby controlling the bandgap and CBO with the absorber layer effectively (Delft et al., 2012; Hong et al., 2016; Kobayashi et al., 2013; Törndahl et al., 2007). Till date, several ALD-grown binary as well as ternary buffer layers such as ZnSe (Ohtake et al., 1995), ZnO (Chaisitsak et al., 1999, 2000; Malm et al., 2005; Platzer-Björkman et al., 2003c; Shimizu et al., 2000), Zn(O, S) (Hultqvist et al., 2009, 2011; Illiberi et al., 2018; Kobayashi et al., 2013; Larsson et al., 2018; Nakashima et al., 2012; Platzer-Björkman et al., 2003b, 2006), ZnMgO (Hultqvist et al., 2009; Pettersson et al., 2009; Platzer-Björkman et al., 2007; Törndahl et al., 2009, 2007), ZnSnO (Agbenyeke et al., 2018; Hultqvist et al., 2011a, 2012, Lindahl et al., 2013a, 2013b, 2016; Salomé et al., 2017), In_2S_3 (Abou-Ras et al., 2005; Guillemoles et al., 2001; Naghavi et al., 2003; Spiering et al., 2004, 2003, 2005; Sterner et al., 2005; Yousfi et al., 2000, 2001), *etc.* have exhibited a remarkable progress in chalcopyrite-type TFSCs owing to their tunability in bandgap *via* compositional control to achieve favorable CBO and a reduction in carrier recombination at the absorber/buffer interface.

3. ALD-grown buffer layers for Cu(In,Ga)Se_2 (CIGS)-based TFSCs

Copper indium gallium diselenide [Cu(In,Ga)Se_2; CIGS] is the most established chalcopyrite-type absorber material to realize a TFSC with high *PCE*. Recently, CIGS-based TFSCs have exhibited a record *PCE* of >20% (Green et al., 2017; Jackson et al., 2016; Menner et al., 2017) with a conventional film stack such as soda lime glass (SLG)/Mo/CIGS/buffer layer/window layer (mostly i-ZnO/Al:ZnO) with a metal contact (Fig. 2a). A CIGS absorber layer with a bandgap of 1–1.7 eV (Bakke et al., 2011; Farhadi and Naseri, 2016; Hultqvist et al., 2011a, 2011b) is generally grown by physical vapour phase deposition techniques such as co-evaporation (Hultqvist et al., 2011a; Jackson et al., 2015; Repins et al., 2008), molecular beam epitaxy (MBE) (Kobayashi et al., 2013; Tokio and Masayuki, 2002), *etc.* The CBD-grown CdS is the most common buffer layer that yielded these highest performances in CIGS-based TFSCs. However, this standard device structure with most favorable CBD-CdS buffer layer still suffers dominant recombination mechanism, which induces the bucking current that results in a reduction in V_{oc}. For a chalcopyrite-based TFSC, like CIGS, with a *p-type* absorber usually has the Fermi-level (E_f) at the interface close to the conduction band and the minority carriers of the bulk absorber layer are considered as majority carriers at the interface, which should not be recombined significantly. Therefore, the performance of an ideal heterojunction TFSC is almost independent from the interface recombination velocity. In contrast, a different situation occurs owing to the unfavorable band alignment at the absorber/buffer interface. According to the general assumption, a small spike (positive CBO) formation at the interface is beneficial for the increasing trend of the inversion that helps in reduction of the interface recombination. Thus, a moderate spike formation does not affect the V_{oc} and the current collection. On the other hand, a cliff (negative CBO) formation is detrimental to the type inversion that creates the recombination path by decreasing the barrier at the interface. Nevertheless, a detail description about these band alignments can be found elsewhere (Sinha et al., 2018a). A spike CBO formation within the range of 0–0.4 eV at the CIGS/buffer interface is usually favorable to achieve high device performance, leading to an constant V_{oc} without affecting the short circuit current density (J_{sc}) (Minemoto et al., 2001; Siebentritt, 2004), while, higher than 0.4 eV CBO (cliff) formation reduces the device performances. The CBD-CdS buffer usually forms the spike CBO at the interface with CIGS absorber with the value ranging from 0 to 0.4 eV that reveals an excellent device performance. Such a spike CBO formation is comparatively easy for the standard CIGS absorber with low bandgap, while this could be difficult for wide bandgap absorbers, where cliff CBO formation occurs for CdS buffer (Nadenau et al., 2000; Siebentritt, 2004). Therefore, the alternative buffers are expected to form higher CBO with such wide bandgap chalcopyrite absorber-based TFSCs to obtain better performances. According to the literature, a low defect density is desirable at the absorber/buffer interface to reduce Fermi level pinning, which further enhance the inversion and improve the V_{oc} of the devices (Klenk, 2001; Naghavi et al., 2010; Rau et al., 1999). Beside an advantage of CdS over other materials owing to its lattice matching during low temperature epitaxial growth, a significant interface defects density could be observed at a typical growth process (Furlong et al., 1998). Furthermore, a comparatively narrow bandgap of 2.4–2.5 eV of the CdS buffer layer induces parasitic absorption that restricts the device efficiency, especially in the short wavelength region (Naghavi et al., 2010).

Therefore, to overcome its drawbacks, extensive research efforts were initiated to replace CdS (Naghavi et al., 2010). Accordingly, ALD was found to be compatible with the CIGS growth process for deposition of Cd-free materials, and there are a number of research studies concerned with Cd-free ALD-grown buffer layers to realize a CIGS-based

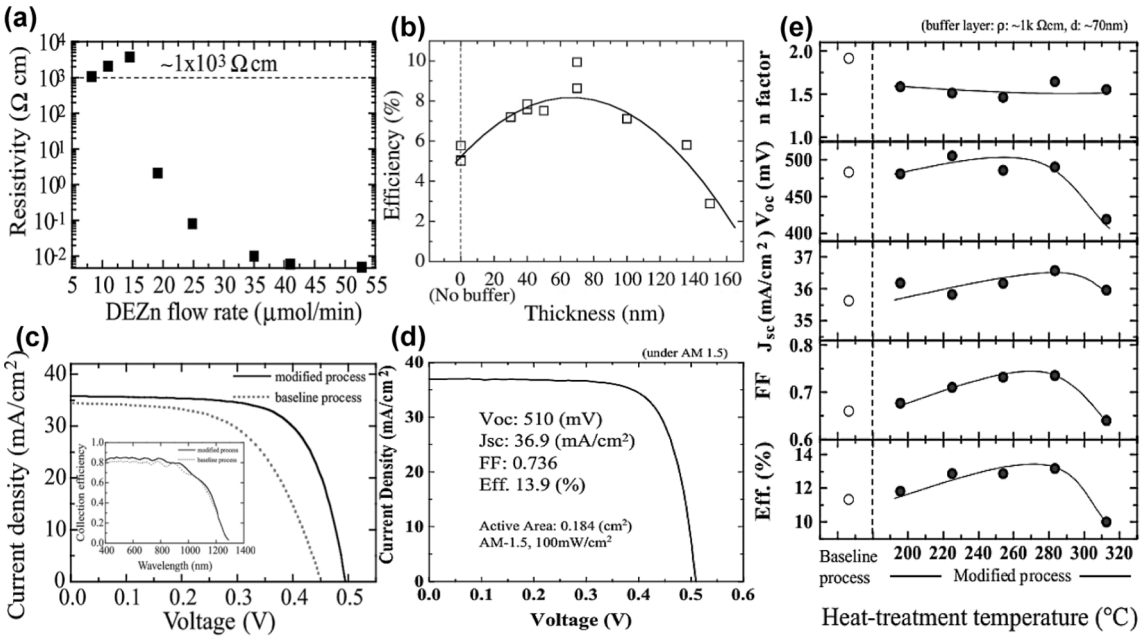

Fig. 3. (a) Resistivity of un-doped ALD-ZnO films as a function of the DEZ flow rate, (b) *PCE* versus buffer layer thickness, and (c) illuminated *J–V* characteristics (spectral response shows in the inset) of cells fabricated by different buffer layer growth processes. [Reprinted with permission from Chaisitsak et al. (Chaisitsak et al., 1999) Copyright 1999, The Japan Society of Applied Physics]. (d) *J–V* curve of a CIGS/ZnO solar cell with an i-(ALD)-ZnO buffer layer and (e) solar cell parameters versus heat-treatment temperature (The straight line is for visual guide). [Reprinted with permission from Chaisitsak et al. (Chaisitsak et al., 2000) Copyright 2000, The Japan Society of Applied Physics].

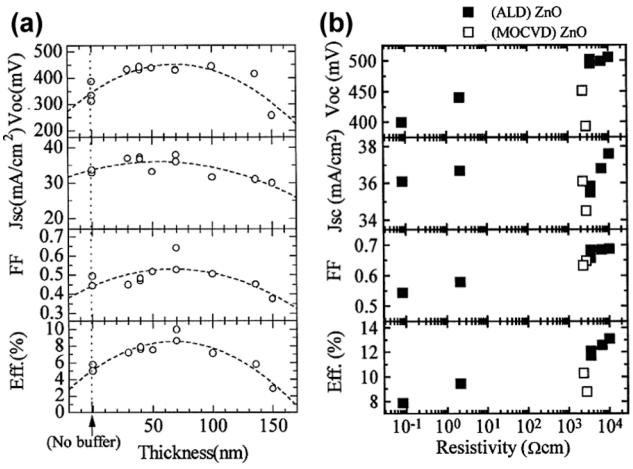

Fig. 4. Solar cell parameters as functions of the buffer layer (a) thickness and (b) resistivity. [Reprinted with permission from Shimizu et al. (Shimizu et al., 2000) Copyright 2000, Elsevier].

TFSCs with a high *PCE* (Fig. 2b). A further discussion on such devices is included in the following sections.

3.1. ZnSe

The earliest report on ALD-grown Zn-based buffer layer was published in 1995 by Ohtake et al. (Ohtake et al., 1995). Though diethylzinc [$Zn(C_2H_5)_2$; DEZ] is now considered as common ALD-precursor for depositing all Zn-based buffer layers, in this very first attempt, ZnSe was deposited by alternate exposures of elemental Zn and Se for a polycrystalline CIGS-based TFSC to study the solar cell performance in detail for different thicknesses of ZnSe buffer. It demonstrated the capability of ALD to deposit a buffer layer of thickness up to 1 nm precisely while achieving a fill factor (*FF*) comparable with a CdS-based buffer layer. In addition, they further established the superiority of ALD process over co-evaporation, which is another popular gas phase deposition technique widely used to grow a buffer layer. It should be noted that the highest *PCE* achieved by the ALD-grown ZnSe buffer layer (10-nm-thick) for a CIGS TFSC was as high as 11.6%, which was higher compared with co-evaporation (9%).

3.2. ZnO

A couple of years after the first attempt to deposit a ZnSe buffer layer by ALD, few attempts were made to grow ZnO as another Zn-based binary buffer layer for CIGS TFSC (Chaisitsak et al., 1999, 2000; Malm et al., 2005; Platzer-Björkman et al., 2003c; Shimizu et al., 2000). The intent behind the oxide-based buffer layer was to make the CIGS cell free of both Cd and S. In the very first report of Chaisitsak et al. (Chaisitsak et al., 1999) investigated the performance of CIGS TFSCs with ZnO buffer layer of variable resistivity, which was obtained by varying the flow rate of DEZ (ALD precursor) during the course of deposition (Fig. 3a), in addition to the variable buffer layer thicknesses. A high-resistivity ($>10^3$ Ω-cm) and transparent (>80%) ALD-grown ZnO buffer layer with an optimized thickness of 70 nm (Fig. 3b) resulted in a maximum cell performance as a possible consequence of reduced recombination at/near the CIGS/ZnO heterojunction owing to the resistive buffer layer (Olsen et al., 1996). This study also proposed a modified process for further performance enhancement of a TFSC by heat treating the CIGS absorber layer before depositing the ZnO buffer layer by ALD. Fig. 3c shows significant enhancement in both V_{oc} and *FF* achieved using the modified process with a maximum *PCE* of 12.1% for an optimized TFSC without anti-reflection (AR) coating. During a more detail study on the effect of surface treatment (Chaisitsak et al., 2000), achieved an enhanced *PCE* of 13.9% (Fig. 3d) using a modified process in which the CIGS surface was subjected to heat treatment that helped remove entities, like excess In_xS_y, from the surface to avoid the inter-diffusion into the buffer and TCO layer and thereby improve the performance of the device (Fig. 3e) up to an optimized temperature. In addition, the investigation on reversible light soaking effect showed a further improvement in *PCE*, which revealed the origin of the effect may

be at/near the CIGS surface or grain boundaries that affect the cell performance only because of the formation of the junction with ZnO buffer layer. In another report by Shimizu et al. (Shimizu et al., 2000), also focused on the optimization of resistivity and thickness of the ALD-grown buffer layer, achieved a high CIGS cell *PCE* of 13.2% (Fig. 4a) for 75-nm-thick ZnO layer. Similar to the previous report by Chaisitsak et al. (Chaisitsak et al., 1999), this study also revealed that a high-resistivity ($>10^3$ Ω-cm) of ZnO buffer could provide a high V_{oc} and a high *FF* (Fig. 4b) without affecting the J_{sc} of the cell. Unlike in the CdS buffer layer, a reversible conventional light soaking effect was also evidenced, while a light soaking for ~1 h significantly increased (~64%) the *PCE* of the CIGS TFSC. Quite surprisingly the other two relatively recent articles, which were published after the earlier study discussed in this section, observed much less *PCE* for an ALD-grown ZnO buffer layer. The work by Platzer-Björkman et al. in 2003 and by Malm et al. in 2005 reported the *PCE* for CIGS TFSCs with ALD-grown buffer layer as 5–8% after annealing and 4.5%, respectively (Malm et al., 2005; Platzer-Björkman et al., 2003c). Regarding the ALD-grown ZnO buffer layer in CIGS, the low *PCE* is attributed to a negative CBO ($\Delta E_c = -0.2 \pm 0.2$ eV) at the CIGS/ZnO interface which leads to a considerable voltage loss, up to 200 mV (Platzer-Björkman et al., 2003c). The huge voltage loss results in a significant difference in *PCE* between this ZnO-based cell (~5–8%) with a CdS-based reference cell (14% and 13.5%, respectively) for these two studies. However, the later study, with the help of temperature-dependent *J–V* measurements (*J–V–T*), showed that the interface recombination for both ALD-grown ZnO and CdS are consistent as both of these form a negative CBO at the interface (Malm et al., 2005). Therefore, the reason for such significant difference in *PCE* might be justified by the lack of optimizations in the ZnO thickness or the electrical properties of the ALD-grown ZnO film which helped achieve much higher *PCE* in the earlier studies on ALD-grown ZnO buffer layer for CIGS.

Table 1
Solar cell parameters of devices with Zn(O,S) buffer layers of varying thickness and S concentration. The two bottom lines indicate the solar cell parameters of the best 500-cycle Zn(O,S)10% device and the corresponding CdS reference cell. [Reprinted with permission from Platzer-Björkman et al. (Platzer-Björkman et al., 2006) Copyright 2006, American Institute of Physics].

	V_{oc} [mV]	J_{sc} [mA/cm^2]	*FF* [%]	*PCE* [%]
CdS	575	33.2	73.7	14.1
500 cycles:				
Zn(O,S)5%	439	33.9	44.6	6.6
Zn(O,S)10%	507	33.5	67.1	11.4
Zn(O,S)20%	190	0.1	17.0	0.0
300 cycles:				
Zn(O,S)10%	535	34.8	73.2	13.6
Zn(O,S)20%	542	34.8	71.5	13.5
Zn(O,S)33%	545	34.8	43.9	8.3
100 cycles:				
Zn(O,S)20%	418	33.4	66.8	9.3
Zn(O,S)33%	478	35.1	68.8	11.5
ZnS	522	34.6	62.9	11.3
Zn(O,S)10%	642	34.3	74.4	16.4
CdS	624	33.3	75.8	15.8

It was clear that an ALD-grown pristine ZnO cannot provide a positive CBO as the band gap of ZnO cannot be varied. Therefore, Zn-based ternary compounds were attempted as the alternative buffer layers, which can help control the bandgap of the material and hence the CBO at the CIGS/buffer layer interface. ALD can probably be considered the most efficient technology to control the composition of a ternary material in the most precise way. Eventually, these two facts drove the research to explore the possibilities with different ALD-grown Zn-based ternary buffer materials for CIGS-based TFSCs.

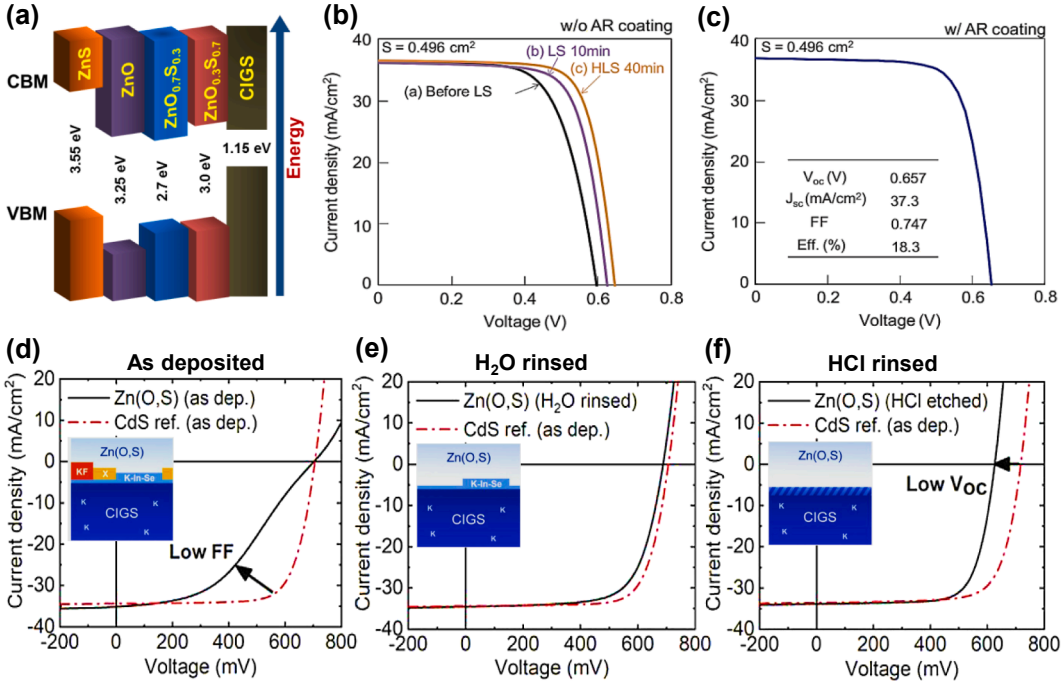

Fig. 5. (a) Schematic band diagrams of the CIGS/Zn(O,S), CIGS/ZnO, and CIGS/ZnS interfaces. (b) *J–V* characteristics of ZnO:B/ZnO/Zn(O,S)/CIGS solar cells before and after one-sun light soaking for 10 min and subsequent heat-light soaking for 40 min, with the Zn(O,S) layer deposited at a $H_2S/(H_2O + H_2S)$ pulse ratio of 0.27 and (c) *J–V* characteristics of the best CIGS solar cell fabricated with a 50-nm-thick ALD-grown Zn(O,S) buffer layer. [Reprinted with permission from Kobayashi et al. (Kobayashi et al., 2013) Copyright 2013, Elsevier]. Representative *J–V* curves for Zn(O,S) devices fabricated with CIGS-KF (d) as deposited, (e) after water rinsing, or (f) after HCl (2 M) etching. CdS reference devices fabricated with as-deposited CIGS-KF are included. The schematic pictures qualitatively show the surface phases on the CIGS-KF surface after the different surface treatments. The phase labelled "X" represents a gallium- and fluorine containing salt. The dashed region on the etched sample indicates a potassium-depleted surface region and possibly an HCl-modified surface. [Reprinted with permission from Larsson et al. (Larsson et al., 2018) Copyright 2018, Elsevier].

3.3. Zn(O,S)

The first study on the ALD-grown Zn-based ternary buffer layers considered Zn(O,S), where Zn(O,S) was deposited by ALD at 120 °C using a DEZ-H_2O (for ZnO) and a DEZ-H_2S (for ZnS) system with 20% S (Platzer-Björkman et al., 2003b). They obtained a high *PCE* of 16% by using an ALD-grown Zn(O,S)/ZnO bilayer buffer layer. However, this attempt on ALD-grown Zn(O,S) buffer layers was the very first of its kind, and there were some issues with reproducibility of buffer layer due to the differences in the CIGS surfaces (Platzer-Björkman et al., 2003a). The researchers observed an incomplete coverage of the thin Zn(O,S) buffer layer on the CIGS surface, which was finally successfully overcome by using a longer ALD pulse time for all the precursors (DEZ, H_2O, and H_2S) and obtained a *PCE* of 12.1% without AR coating. A further study (Platzer-Björkman et al., 2006) exhibited the effect of S concentration in the ALD-grown Zn(O,S) buffer layers in CIGS in terms of the band alignment at the CIGS/Zn(O,S) interface, which usually determines the cell performance. It was observed that the V_{oc} of the cell was significantly low at no or small S concentration (up to $ZnO_{0.7}S_{0.3}$) owing to the negative CBO (−0.2 eV) with a cliff formation at the interface. On the other hand, a pure ALD-grown ZnS buffer layer showed a very low J_{sc} caused by a very large CBO (spike formation) at the interface. Fig. 5a shows the band alignment with pure ZnO and ZnS layers and at two different stoichiometry of Zn(O,S) in CIGS. This illustration helps realize the cliff and spike formations in these buffer layers. The systematic study of the solar cell parameters with different S concentrations of Zn(O,S) deposited with different ALD cycles are shown in Table 1, where a highest *PCE* of 16.4% was observed with the Zn(O,S) buffer layer as compared to the 15.8% obtained using the CdS-based standard buffer layer. In contrast, Hultqvist et al. (Hultqvist et al., 2011b) reported an interesting study on ALD-grown Zn(O,S) buffer layers with different Zn to S ratios in CIGS TFSCs with different contents of Ga (x = 0.3, 0.5, and 0.75 in $CuIn_{1-x}Ga_xSe_2$). It was shown that the similar Zn(O,S) yielded the best device performance for different contents of Ga in the absorber. Similar to the previous studies, the varying S content led to similar results where the increasing S content resulted in a higher V_{oc} of the cell due to the positive CBO developed at the interface. The highest *PCE* achieved in this study on $CuIn_{1-x}Ga_xSe_2$ (x = 0.5) was 11.5% (comparable with a CdS reference cell), however, which was much lower than the values reported in other studies. Similar observations (represented by both S/(S + O) or $H_2S/(H_2S + H_2O)$) of the cliff and spike configurations of the CBO for different S to O ratios were made by Kobayashi et al. (Kobayashi et al., 2013). The detailed experiments were carried out on the light soaking of Zn(O,S) buffer layers. It was found that a light soaking at room temperature followed by a heat-light soaking (HLS) improved the performance of the cell. Significant increases in the V_{oc}, *FF*, and *PCE* were observed at an optimized light soaking of 10 min

Table 2
Average (and best) *J–V* parameters for CIGS-KF/Zn(O,S) devices fabricated using the etch-and-anneal approach, and the corresponding CIGS-KF/CdS references. CIGS-KF/CdS reference devices without HCl etching are included for a more detailed comparison. [Reprinted with permission from Larsson et al. (Larsson et al., 2018) Copyright 2018, Elsevier].

Buffer Layer	Pre-ALD treatment	J_{sc} [mA/cm^2]	V_{oc} [mV]	*FF* [%]	*PCE* [%]
Zn(O,S)	HCL (2 M)	33.7 (34.3)	619 (626)	72.5 (73.2)	15.1 (15.5)
Zn(O,S) annealed 165 °C, 30 min	HCL (2 M)	34.6 (34.9)	692 (696)	73.8 (74.1)	17.7 (18.0)
Zn(O,S) annealed 180 °C, 60 min	HCL (2 M)	34.3 (34.9)	689 (692)	74.1 (74.5)	17.5 (17.9)
CdS	HCL (2 M)	32.9 (33.3)	692 (695)	73.0 (73.6)	16.6 (16.8)
CdS annealed 180 °C, 60 min	HCL (2 M)	33.4 (33.7)	696 (699)	74.5 (74.9)	17.3 (17.6)
CdS	None	33.1 (33.6)	715 (718)	73.3 (74.1)	17.3 (17.8)
CdS annealed 180 °C, 60 min	None	33.9 (34.3)	707 (713)	74.3 (75.5)	17.8 (18.3)

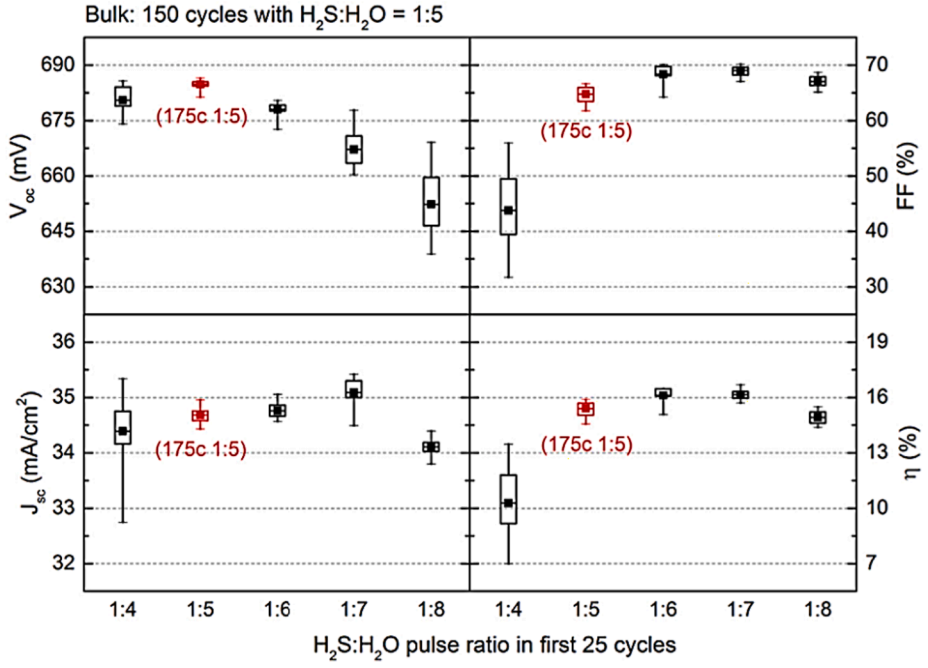

Fig. 6. Trends in V_{oc}, *FF*, J_{sc}, and η (*PCE*) for Zn(O, S) devices where the $H_2S:H_2O$ pulse ratio was varied during the first 25 ALD cycles. Those cycles were followed by 150 cycles of the baseline 1:5 process. The CIGS-KF absorbers were rinsed in water prior to ALD. The red data correspond to the baseline 1:5 process (for all 175 cycles). [Reprinted with permission from Larsson et al. (Larsson et al., 2018) Copyright 2018, Elsevier].

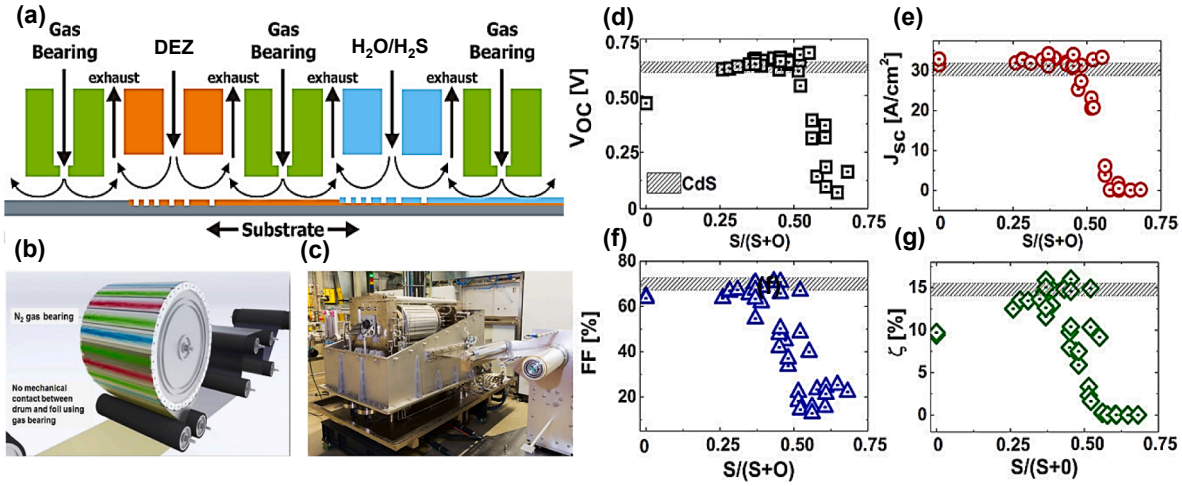

Fig. 7. (a) Schematic of a laboratory-scale rotary spatial-ALD reactor. The DEZ and H_2O/H_2S half-reaction zones are separated by gas bearings. [Reprinted with permission from Illiberi et al. (Illiberi et al., 2012) Copyright 2012, American Chemical Society] (b) Schematic of the roll-to-roll spatial-ALD concept, consisting of a central rotating drum that contains ALD precursors, which are separated and surrounded by nitrogen gas bearings. (c) A picture of the roll-to-roll spatial-ALD setup built by the VDL Enabling Technology Group. Photovoltaic parameters of CIGS TFSCs ($S = 0.52$ cm^2) on glass where S-ALD Zn(O,S) layers with different S/(S + O) ratios are used as buffer layers: (d) V_{oc}, (e) J_{sc}, (f) *FF*, and (g) *PCE* (ζ) vs. S/(O + S) ratio. The patterned area in each graph represents the values of the photovoltaic parameters for cells with a CdS buffer layer grown by CBD. [Reprinted with permission from Illiberi et al. (Illiberi et al., 2018) Copyright 2018, American Vacuum Society].

followed by a HLS for 40 min, as shown in Fig. 5b. The highest *PCE* (18.3%) till that date for CIGS TFSCs with ALD-grown Zn(O,S) buffer layers was achieved (with an AR coating of MgF_2) (Fig. 5c) owing to the moderate spike formation (CBO ~0.36 eV) at the CIGS/Zn(O,S) interface, which attributed to the high V_{oc} by reducing the interface recombination.

In a most recent time, a completely different type of investigation by Larsson et al., explored the effect of several systematic wet-chemical post-deposition treatments (PDT) of the CIGS surface such as a KF treatment followed by either a rinsing with H_2O or an etching with diluted HCl especially prior to deposition of ALD-Zn(O,S) buffer layer (Larsson et al., 2018). A beneficial effect on V_{oc} was observed, irrespective of buffer layer material, owing to the KF PDT of the CIGS surface (CIGS-KF). In contrast, a severe blocking behaviour with a low *FF* was revealed for the CIGS-KF/Zn(O,S) devices, which restricted the device *PCE* to 10.7% ($V_{oc} = 703$ mV, $J_{sc} = 35.2$ mA/cm^2, $FF = 43.4\%$) compared to the *PCE* of 18% ($V_{oc} = 706$ mV, $J_{sc} = 34.4$ mA/cm^2, $FF = 74.2\%$) for a CIGS-KF/CdS reference device (Fig. 5d). A significant improvement in diode quality was obtained for CIGS-KF/Zn(O,S) devices with an increased *PCE* of 16.5% ($V_{oc} = 688$ mV, $J_{sc} = 34.6$ mA/cm^2, $FF = 69.2\%$), when the CIGS-KF substrates were rinsed with H_2O to remove the salts on surface before ALD of Zn(O,S) (Reinhard et al., 2015). However, the H_2O-rinsed CIGS-KF/Zn(O,S) device still suffered from a lower *FF* due to K-In-Se rich CIGS surface, which possibly hindered the nucleation of Zn(O,S) ALD process (Fig. 5e). On the other hand, the V_{oc} was considerably decreased for the CIGS-KF/Zn(O,S) device compared to that of the reference device, CIGS-KF/CdS, when the CIGS-KF surface was treated with diluted HCl (Fig. 5f) before ALD of Zn(O,S). Furthermore, the Zn(O,S) ALD on H_2O rinsed KF-treated CIGS surface was investigated by using a two-step ALD with different S:O (controlling H_2S:H_2O ration) ratio, which showed a remarkable effect on the device characteristics when the ratio was varied between 1:4 and 1:8 for the initial 25 cycles of ALD, while it was kept constant at 1:5 during the subsequent 150 cycles in the bulk regime (Fig. 6). The V_{oc} decreased with the increasing H_2O pulse, whereas the average *FF* increased. The opposite nature of V_{oc} and *FF* attributed to the change in CBO from spike to cliff like junction at the absorber/buffer interface.

Alternatively, when S:O ratio was varied during the 150 ALD cycles in the bulk regime and held constant at 1:5 during the first 25 cycles, a blocking behaviour of *J–V* characteristics and lower V_{oc}, J_{sc}, and *FF* were observed for Zn(O,S) buffer (S:O = 1:4) with a high S content due to the high conduction band energy in the bulk Zn(O,S). On the other hand, the V_{oc} was reduced with the decrease in S content (S:O = 1:6) associated with a lowered conduction band energy of the bulk Zn(O,S) buffer layer. The two-step Zn(O,S) ALD with a controlled S:O ratio (initial 25 cycles with 1:6, followed by 150 cycles with 1:5) revealed an average *PCE* of 16.8% ($V_{oc} = 690$ mV, $J_{sc} = 35.1$ mA/cm^2, $FF = 69.5\%$) for the H_2O-rinsed CIGS-KF absorbers in comparison to 17.7% for the CdS-based reference ($V_{oc} = 711$ mV, $J_{sc} = 34.5$ mA/cm^2, $FF = 72.3\%$). Furthermore, the reduction in V_{oc} owing to the removal of K-In-Se rich CIGS-KF surface phase using diluted HCl etching was regained by a post-annealing of the device at a low temperature (Table 2).

Apart from the vacuum-based conventional ALD, recently, Illiberi et al. (Illiberi et al., 2018), introduced a spatial ALD (S-ALD) that deposits Zn(O,S) buffer layer under atmospheric pressure for both rigid as well as flexible CIGS TFSCs, where they also demonstrated large-scale integration of flexible modules with an area of 270 cm^2 with Zn(O,S) buffer layer using a roll-to-roll S-ALD that uses DEZ and H_2O/H_2S mixture (Fig. 7a–c). A higher J_{sc} was obtained with Zn(O,S) buffer layer for $0 < S/(S + O) < 0.5$ in comparison with a reference device with CdS buffer layer due to the wider bandgap of Zn(O,S) that lowered the absorption losses in the blue wavelength region. Similarly, the V_{oc} was also increased with the increase in S concentration, and it reached a value that was comparable to the reference cell for S/(S + O) ~0.4. According to the author, this was attributable to the passivation effect of S atoms at

Table 3
Device characteristics of record solar cells with the S-ALD Zn(O,S) buffer layer. [Reprinted with permission from Illiberi et al. (Illiberi et al., 2018) Copyright 2018, American Vacuum Society].

Buffer layer	Substrate	J_{sc} [mA/cm^2]	V_{oc} [mV]	*FF* [%]	*PCE* [%]
CBD CdS	Glass 30 × 30 cm^2	32.1	665	72.7	15.5
Laboratory scale S-ALD Zn(O,S)	Glass 15 × 15 cm^2	34.2	662	70.4	15.9
Laboratory scale S-ALD Zn(O,S)	Polyamide 15 × 15 cm^2	32.8	652	61.2	13.1
Roll to role S-ALD ZnOS	Polyamide 50 cm wide	30.1	563	60.0	10.2

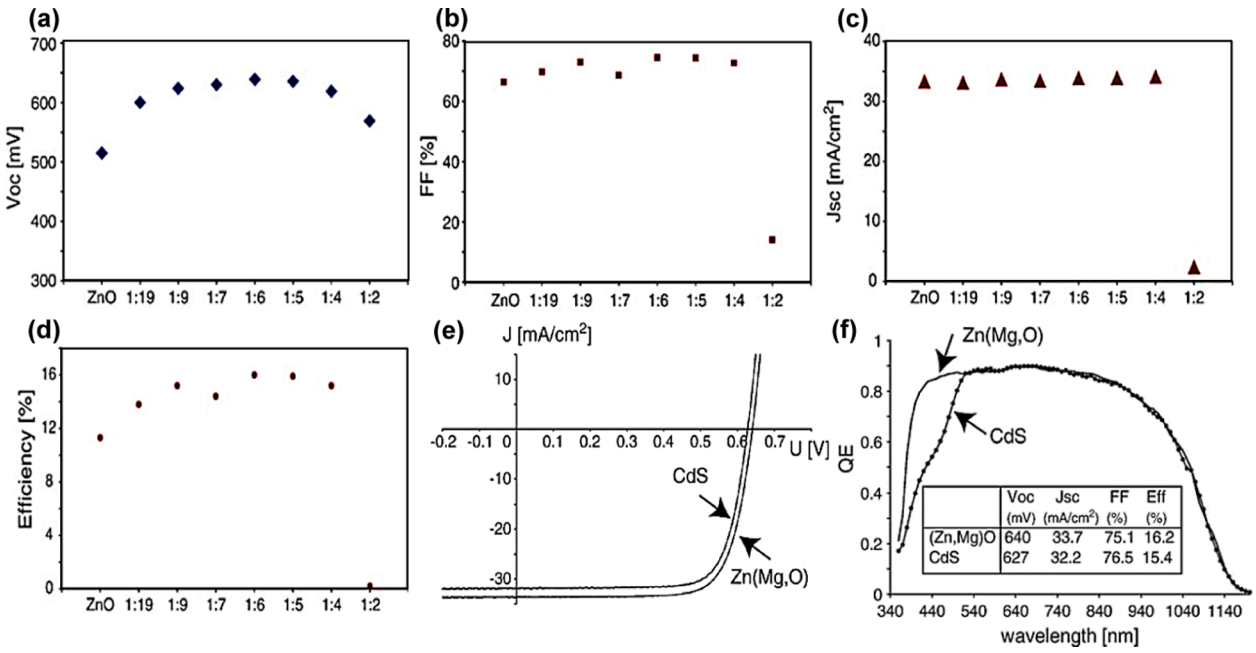

Fig. 8. Average solar cell parameters of devices with ZnMgO buffer layers: (a) V_{oc}, (b) *FF*, (c) J_{sc}, and (d) *PCE* at varying Mg contents deposited using 1000 cycles at 120 °C. (e) *J–V* and (f) external quantum efficiency (EQE, λ) characteristics and solar cell parameters of the best device with a ZnMgO buffer layer (1:6 process with 1000 cycles) as compared to the CdS reference device. [Reprinted with permission from Platzer-Björkman et al. (Platzer-Björkman et al., 2007) Copyright 2007, Elsevier].

the CIGS/Zn(O,S) interface. Subsequently, a further increase in S/(S + O) ratio (>0.5) led to the formation of a high potential barrier at the interface, which resulted in a drastic decrease in all cell parameters (Fig. 7d–g) because the electron transport was blocked. The best *PCE* of 15.9% (V_{oc} = 662 mV, J_{sc} = 34.2 mA/cm^2, *FF* = 70.4%) was achieved for the Zn(O,S) buffer layer [S/(S + O) ratio of ~0.4] compared to 15.5% (V_{oc} = 665 mV, J_{sc} = 32.1 mA/cm^2, *FF* = 72.7%) of the reference TFSC with CdS buffer layer. Furthermore, the S-ALD was also applied to deposit Zn(O,S) buffer layers on flexible CIGS TFSCs in both the laboratory-scale and roll-to-roll systems. The detailed device parameters of the flexible CIGS TFSCs and mini-modules along with the TFSCs on glass substrates are tabulated in Table 3. A record *PCE* of 13% was obtained for a flexible CIGS TFSC (S = 0.57 cm^2) with Zn(O,S) buffer layer grown by S-ALD in a laboratory scale system. On the other hand, a best *PCE* of 10.2% was achieved by the roll-to-roll S-ALD of a ZnOS buffer layer on a 50-cm-wide CIGS substrate, while 9.2% was achieved for a mini-module area of 270 cm^2. This study exhibits a new low-cost and large-area TFSCs fabrication process using the atmospheric roll-to-roll S-ALD.

The above discussions reveal that the ALD-grown Zn(O,S) buffer layer works much better than the Zn-based binary materials (ZnSe and ZnO) in CIGS TFSCs. The main advantage of the Zn-based ternary material is to control the CBO for varying bandgap by changing the S/Zn ratio as shown in Fig. 5a. This also helps optimize the electrical and optical properties of such buffer materials. Therefore, research focus is moved forward in search of new ternary buffer layers, where other binary oxides combine with ZnO. In this context, we find the ALD-grown ZnMgO and ZnSnO buffer layers as discussed in the following sections.

3.4. ZnMgO

In 2007, Törndahl et al. (Törndahl et al., 2007) explored zinc magnesium oxide (ZnMgO) as another Zn-based ternary buffer layer for CIGS TFSCs. A variable stoichiometric ratio of Zn to Mg was followed to deposit the layer in the form of ZnMgO using DEZ, bis-cyclopentadienyl magnesium [$Mg(C_5H_5)_2$ or $MgCp_2$], and H_2O as the precursors. A controlled composition (x, for $Zn_{1-x}Mg_xO$) of the buffer layer was achieved by controlling the amount of Mg precursor as well the deposition

Table 4
J–V parameters of devices with $Zn_{1-x}Mg_xO$ buffer layers deposited on CIGS absorbers by 1000 ALD cycles at different temperatures, and optical energy bandgap and resistivity for $Zn_{1-x}Mg_xO$ buffer layers grown on the glass at the same time. [Reprinted with permission from Törndahl et al. (Törndahl et al., 2009) Copyright 2009, John Wiley and Sons].

ZnMgO T_{dep} [°C]	V_{oc} [mV]	J_{sc} [mA/cm^2]	*FF* [%]	*PCE* [%]	$Zn_{1-x}Mg_xO$ process	E_g [eV]	Resistivity [Ω-cm]
105	622	31.6	72.0	14.1	1:9	3.52	40
120	639	32.6	74.5	15.5	1:6	3.62	110
135	604	32.1	72.3	14.0	1:4	3.72	72
150	485	31.9	46.2	7.15	1:4	3.64	7.4
180	470	31.3	48.4	7.12	1:4	3.62	0.61
CdS	626	31.6	75.7	15.0	–	–	–

temperature within a range of 105–180 °C, which revealed a *PCE* as high as 14.1% using an ALD-grown ZnMgO buffer layer in a CIGS TFSC, and this was much higher than that achieved with a CdS buffer layer (13.7%). However, a lower V_{oc} was obtained compared to that of CdS reference cells, which was not observed for the Zn(O,S) buffer. This could be owing to the more passivation ability of S, rather than non-optimized band alignment, which passivate the traps at the interface and thereby improve the V_{oc} of the CIGS TFSCs with ALD-grown Zn(O,S) buffer compared to devices with ZnMgO buffer. Further, more detailed investigation resulted in a higher *PCE* of 16.2% with ALD-grown ZnMgO buffer layer by using a 1:6 ratio for Mg and Zn at 120 °C with an optimum thickness (1000 ALD cycles), though the results showed an independent nature to thickness of buffer layer between 80 and 600 nm (Platzer-Björkman et al., 2007). A bandgap of 3.6 eV was found to be optimized for the maximum reported *PCE*, while the bandgap usually increases due to the incorporation of Mg in the film as reported in the previous study (Törndahl et al., 2007). However, a very high concentration of Mg (Mg:Zn = 1:2) caused a drastic decrease in J_{sc} and thereby V_{oc}, *FF*, and *PCE* due to the blockage of current by a large CBO. A systematic comparison between pure ZnO and ZnMgO buffer layers with increasing Mg concentration was made in this study, as illustrated in

Fig. 8a–d. A further comparison of this ALD-grown buffer layer with CdS unequivocally established the potential of such techniques towards developing TFSCs free of Cd and S (Fig. 8e and f). In continuation of the previous study, an extensive investigation on light soaking followed by temperature dependent current density–voltage measurements (*J–V–T*) indicated that the predominant performance losses for ALD-grown ZnMgO buffer were probably due to interfacial recombination at a low Mg content, while the tunnelling-enhanced recombination mostly took place in the space charge region at a high Mg content (Pettersson et al., 2009). A notable enhancement in device performance is quite obvious for this kind of TFSCs owing to its strong metastable behaviour. It was noticed that light soaking enhanced the V_{oc} of the cell in the case of a pure ZnO buffer layer, while the *FF* was the main parameter influenced in the case of the ZnMgO buffer layers. According to them, the devices with Mg-rich ZnMgO buffer exhibited the low *FF* before light soaking probably because of the positive CBO formation at the CIGS/ZnMgO interface, which is in-line to the previous observation. Conversely, an improvement in *FF* after light soaking could be owing to the persistent photoconductivity (PPC) effect in the buffer layer that possibly lowered that interface barrier by illumination (Eisgruber et al., 1998; Pudov et al., 2005). In this study, the light soaking helped increase the *PCE* of the CIGS TFSCs from 15.3 to 16.1% using an ALD-grown ZnMgO buffer layer. The temperature of ALD to deposit ZnMgO buffer layers also revealed a significant effect on the performance CIGS TFSCs (Platzer-Björkman et al., 2007; Törndahl et al., 2009). It was evidenced that the cell performance started degrading beyond 135 °C, although ZnMgO could be deposited in a temperature range of 105–180 °C (Törndahl et al., 2007). Moreover, huge reductions were observed in the V_{oc} and *FF* of those cells with the buffer layers grown above 150 °C. The study indicated that a direct interface between the absorber and the buffer layer as well as degradation in the ZnMgO buffer layer grown at high temperatures cause a poor cell performance could be due to the decrease in resistivity of the ZnMgO buffer layer. Table 4 presents the solar cell parameters for ZnMgO buffer layers grown at different temperatures along with their corresponding bandgaps and resistivities.

3.5. ZnSnO

Zinc-tin oxide (ZnSnO), another Zn-based ternary oxide, is considered as a promising alternative buffer layer in CIGS TFSCs. ALD has been quite successfully performed to apply this buffer layer in CIGS TFSCs with a precise control over the properties of the material in addition to the pure ZnO to pure SnO_x (Agbenyeke et al., 2018; Hultqvist et al., 2011a, 2012, Lindahl et al., 2013a, 2013b, 2016; Salomé et al., 2017). In 2011, Hultqvist et al. (Hultqvist et al., 2011a) reported the first attempt to evaluate an ALD-grown ZnSnO buffer layer in a CIGS [$CuIn_{0.5}Ga_{0.5}Se_2$] absorber using DEZ and tin(IV)t-butoxide [$Sn(C_4H_9O)_4$ or $Sn(OtBu)_4$] as the metal sources and deionized H_2O as the reactant. The ZnSnO was found to be amorphous (Jayaraj et al., 2008; Ko et al., 2007; Moriga et al., 2004; Perkins et al., 2002; Tadatsugu et al., 1994) that offers an additional advantage to reduce the amount of grain boundaries in buffer layer as well as at the absorber/buffer interface, which further helps decrease the related recombination loss by reducing the amount of interface states. A systematic study performed by increasing the Sn concentration in the buffer layer showed the behaviour similar to that of ZnMgO. Beyond a certain Sn limit in the film, the *PCE* and other related parameters of the solar cells started decreasing, while a ratio of 3:8 (3 ALD cycles of ZnO for every 8 cycles of SnO_x) yielded the highest average *PCE* of 13.3%, which was comparable to that of the reference cell with CdS buffer layer (Table 5). The Sn content in the buffer layer affected the V_{oc} of the cell significantly due to the changes in the CBO. However, in this case, the J_{sc} could not be enhanced in the case of the cells with pure ZnO buffer layer. A much lesser optimized thickness was obtained for the ZnSnO (20–30 nm) buffer layer as compared to that of the ZnMgO buffer layer as well as CdS buffer layer (50–70 nm). However, a severe degradation was observed with time in the performance of a CIGS TFSC with a ZnSnO buffer layer probably due to the change at the CIGS/ZnSnO interface; such degradation did not occur with pure ZnO and CdS buffer layers. Light soaking followed by air annealing helped to recover from this degradation to some extent. A further study (Hultqvist et al., 2012) exhibited the maximum *PCE* achieved for the CIGS TFSC with amorphous ZnSnO was 15.3% at a Sn/(Zn + Sn) ratio in the range of 0.15–0.21, which was ~2% higher than their previous report (Hultqvist et al., 2011a) *via* a more controlled ZnSnO ALD chemistry using tetrakis(dimethylamino)tin [$Sn(N(CH_3)_2)_4$], as a new precursor for Sn instead of $Sn(C_4H_9O)_4$, which usually initiates a chemical vapor deposition (CVD) like film growth for SnO_x because of the initiation of continuous decomposition even at an ALD process temperature of 120 °C. Meanwhile, the CdS reference cell used in this study was found to exhibit a *PCE* of 15.1%. A comparative stability study revealed that a thick ZnSnO buffer layer (76 nm) showed superior stable performance not only under room temperature (RT) storage but even under a dry heat (85 °C) atmosphere, unlike the previously mentioned with lower thickness (20–30 nm) (Hultqvist et al., 2011a). A strong light soaking effect is evidently observable for the TFSCs with ZnSnO, which helped in regaining the *FF* of 23.0% to 71.5% and the corresponding *PCE* up to 15.0% from 4.2% within 4 min for the device with a thick buffer layer. This was probably owing to the reduction in barrier in the conduction band as a consequence of photoconductivity effect and thereby increased band bending, which was also mentioned for ALD-ZnMgO buffer layers (Pettersson et al., 2009). However, the increased *FF* was not stable for long time in darkness, while a clear increase in V_{oc} attributed to the cooling effect after the light soaking. In contrast, a the maximum *PCE* achieved by using ZnSnO buffer layers was reported to be 18% using the above mentioned new ZnSnO-ALD chemistry at deposition temperature of 120 °C, the highest *PCE* reported so far with this buffer layer, by performing a detail thickness optimization (~13 nm) of the buffer layer with an Sn/(Zn + Sn) ratio of 0.18 and a bandgap of 3.3 eV (Lindahl et al., 2013a). Interestingly, the buffer layer thickness needed for achieving this *PCE* was much lower compared to the previous reports in which a better performance was obtained with a thicker buffer layer. Similar to ZnMgO, it was found out that the J_{sc} remained independent of the buffer layer thickness while the V_{oc} and *FF* varied significantly with a change in the buffer layer thickness. Such a notable decrease in device performance could possibly be explained by the lower carrier concentration of ZnSnO that resulting in a decrease of the inversion in the top most part of the absorber with increasing thickness of buffer layer and thereby enhance the recombination at the absorber/buffer interface. However, in this case, the J_{sc} was always observed to be higher than that of the CdS reference cell owing to the higher effective bandgap of ZnSnO buffer layer than CdS. This study revealed that the presence of an intrinsic-ZnO layer (i-ZnO) along with the ALD-grown buffer layer slightly only enhanced the *FF* of the CIGS TFSCs with thinner ZnSnO buffer layer probably due to the improved electrical properties of the devices. An enhanced *PCE* of 18.2% was obtained for

Table 5
Average *J–V* parameters of devices with ZnSnO buffer layers deposited by ALD on CIGS at 120 °C and reference device with CdS buffer layer. [Reprinted with permission from Hultqvist et al. (Hultqvist et al., 2011a) Copyright 2011, John Wiley and Sons].

Buffer layer	V_{oc} [V]	J_{sc}(QE) [mA/cm^2]	*FF* [%]	*PCE* [%]
ZnO	0.255	27.8	49.1	3.49
10:8	0.378	26.4	54.8	5.52
6:8	0.504	27.0	54.3	7.41
4:8	0.644	27.5	67.6	12.0
3:8	0.681	27.9	69.8	13.3
2:8	0.686	25.9	64.9	11.6
1:8	0.631	27.2	66.8	11.4
1:11	0.539	26.7	35.3	5.10
SnO_x	0.0593	20.8	31.6	0.383
CdS	0.715	25.9	71.9	13.3

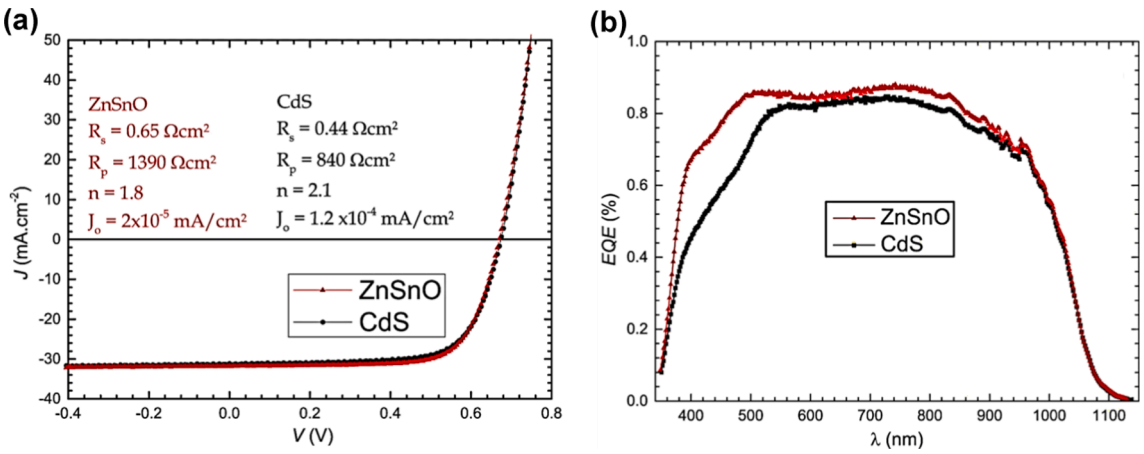

Fig. 9. Electrical characterization of CIGS devices with CdS and ZnSnO buffer layers showing representative curves for (a) *J–V* behaviour and (b) external quantum efficiency. [Reprinted with permission from Salomé et al. (Salomé et al., 2017) Copyright 2017, Elsevier].

CIGS TFSCs with the similar ZnOS-ALD process compared to the 18.6% *PCE* of the CdS reference cell by using a modified inline single-step co-evaporation process to deposit the CIGS absorber layer that exhibited a linear grading in Ga/(Ga + In) profile with an average of ~0.45 in addition to the linear increase in bandgap (1.14 to 1.38 eV) from front to back contact (Lindahl et al., 2013b). A further study by Lindahl et al. (Lindahl et al., 2016) presented the ALD process temperature, with in the range of 90–180 °C (Lindahl et al., 2013a, 2015), dependence performance of CIGS TFSCs with ALD-grown ZnSnO buffer layer by maintaining the [Sn]/([Sn] + [Zn]) composition (~0.169–0.185) and thickness of ZnSnO (48–58 nm on glass substrates) constant with an a decrease in the band gap from 3.74 eV to 3.23 eV, respectively (Lindahl et al., 2015, 2016). The *J–V* characteristics revealed an ALD process temperature window of 105 to 135 °C that resulted in the highest *PCE* of the CIGS TFSCs. The devices with ZnSnO buffer layer deposited at lower temperature (90 °C) was restricted by a poor *FF* due to a roll-over blocking nature. The highest V_{oc} (~672 ± 10 mV) was obtained at a deposition temperature of 105 °C; beyond this temperature, a decrease in the V_{oc} was observed. The same trend was followed by the *FF*, while not much effect was observed on the J_{sc}. Combining the measured *J–V* parameters with the simulated results, it was concluded that the trend of the *J–V* characteristics can be explained by the conduction band line-up theory where a decrease in the ZnSnO bandgap was mostly a result of the change in the conduction band position upon increasing the ALD temperature. Thus, an improved performance was observed when the ALD temperature was in between 90 and 135 °C, owing to a decrease in positive spike-like CBO at the CIGS/ZnSnO interface. The most favorable temperature window was 105–135 °C, which led to the formation of a favorable CBO that resulted in a better performance of the ZnSnO-buffered CIGS TFSCs (*PCE* of 17.3–18.2%) as compared to 17.9% of the CdS reference cell. The performance decreased with a further increase in ALD temperature which resulted in a negative cliff-like CBO. The CIGS TFSCs with the ZnSnO buffer layers deposited at 120 and 150 °C showed activation energies close to the bandgap of CIGS in the

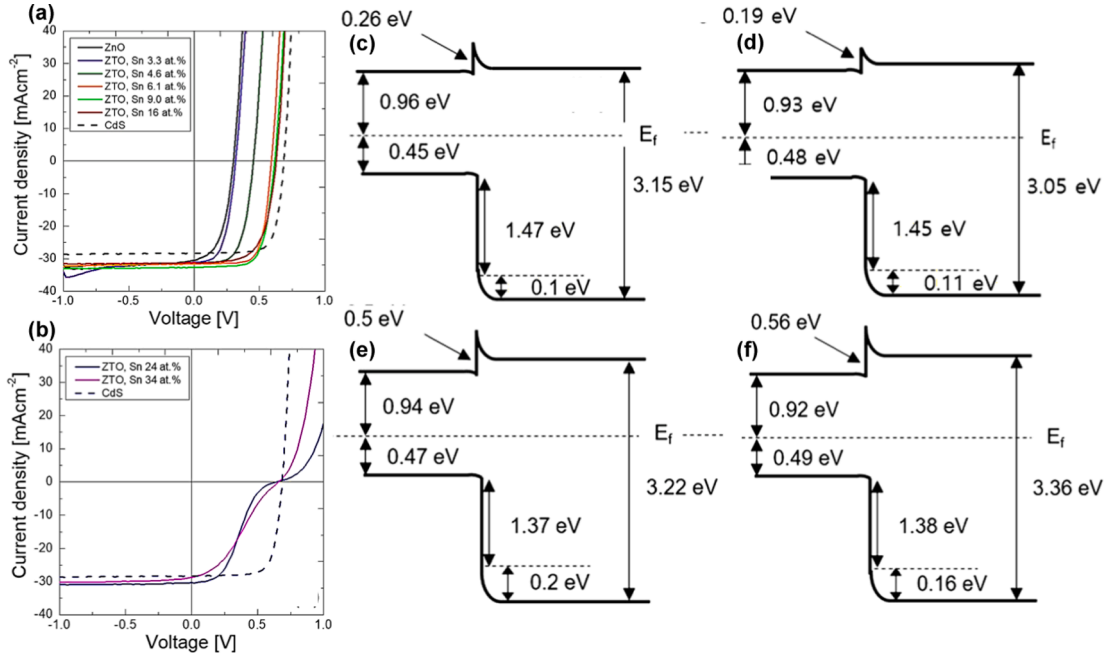

Fig. 10. Illuminated *J–V* curves of (a) ZnSnO films with Sn concentration ≤16 at.% and (b) Sn concentration ≥24 at.% as well as CdS reference cell. Schematic band structure at the CIGS/ZnSnO interface for the different buffer layer compositions of (c) 9 Sn at.%, (d) 16 Sn at.%, (e) 24 Sn at.%, and (f) 34 Sn at.%. [Reprinted with permission from Agbenyeke et al. (Agbenyeke et al., 2018) Copyright 2018, John Wiley and Sons].

Table 6
Effect of In_2S_3 buffer thicknesses on the cell performance. [Reprinted with permission from Yousfi et al. (Yousfi et al., 2000) Copyright 2000, Elsevier].

Buffer	Thickness [nm]	J_{sc} [mA/cm^2]	V_{oc} [mV]	*FF* [%]	*PCE* [%]
Direct ZnO: Al	0	30	466	62.6	8.8
In_2S_3	60	29.6	635	56	10.5
	30	30.6	604	73	13.5
	12	30.5	623	53.5	10.2
	6	29.6	616	43.6	8

temperature-dependent *J–V* measurements, which indicated that the cells were dominated by the Shockley–Read–Hall recombination in the bulk of the absorber (Hegedus and Shafarman, 2004; Rau and Schock,1999). Onthe other hand, an activation energy lower than the absorber bandgap was observed in the cells with the ZnSnO buffer layers deposited at 90 and 180 °C, thus indicating that the recombination at the CIGS/ZnSnO interface due to the large positive and negative values of CBO, respectively, was the most dominant phenomenon (Nadenau et al., 2000; Rau et al., 2004; Turcu et al., 2002). Thus, it was suggested that a low temperature during the ALD of ZnSnO buffer layers is suitable for fabricating a solar cell with a CIGS absorber of large bandgap. Another comparative study between CBD-CdS (50–70 nm) and ALD-grown ZnSnO (20–30 nm) buffer layers for CIGS TFSCs (Salomé et al., 2017) showed almost similar *PCEs* and little higher external quantum efficiency (EQE) for ZnSnO buffer than CdS buffer (Fig. 9) due to higher value of J_{sc} with a wider bandgap of ZnSnO. However, the CIGS/ZnSnO devices suffered from low *FF* and V_{oc} compared to CIGS/CdS devices, which was further attributed to the degradation of series resistance and lower surface photovoltage (CIGS/ZnSnO= ~+164 ± 73 mV and CIGS/CdS= ~+183 ± 55 mV). The key advantage of the ALD-grown ZnSnO buffer layer was the small amount of active defects and low fluctuating potential at the CIGS/ZnSnO interface which further influenced the performance of TFSCs.

Recently, Agbenyeke et al. (Agbenyeke et al., 2018) reported ALD-grown ZnSnO buffer layer for CIGS TFSCs with a tunable bandgap between 3.05 and 3.36 eV by controlling Sn/(Sn + Zn) atomic ratio. According to their report, a 20-nm-thick ALD-ZnSnO buffer layer with different Sn/(Zn + Sn) ratio was deposited on CIGS absorber layer, which exhibited that an Sn concentration of ~9–16 at.% was responsible for the better performance of CIGS TFSCs. Compared with the ZnO buffer layer, a continuous increase in V_{oc} was observed with the incorporation of SnO_2 in the pristine ZnO for an Sn concentration ≤ 16 at.% (Fig. 10a), which resulted in the best *PCE* of 13.9% (at 9 Sn at.%) compared to the 14.4% *PCE* of CdS reference cell due to the change in band position from a cliff to spike-type CBO. On the other hand, for the ZnSnO buffer layer with a higher Sn concentration (>16 at.%) revealed a high energy barrier at the CIGS/ZnSnO interface, which led to a distorted (S-shaped) *J–V* characteristics with lower *FF* and *PCE* (Fig. 10b) by blocking the carrier transport. In addition, they also showed that the performance of the TFSCs was independent of the thickness of the ZnSnO buffer layer for 16 at.% of Sn. Furthermore, a detailed investigation of the band alignment at the CIGS/ZnSnO interface revealed a more spike-type CBO with an increase in Sn concentration in the ZnSnO buffer layer (Fig. 10c–f), which were in good agreement with the obtained *J–V* characteristics.

3.6. In_2S_3

Indium sulfide (In_2S_3) is another ALD-grown buffer layer material, which was investigated extensively by several research groups for CIGS TFSCs (Abou-Ras et al., 2005; Bugot et al., 2018; Guillemoles et al., 2001; Naghavi et al., 2003; Spiering et al., 2004, 2003, 2005; Sterner et al., 2005; Yousfi et al., 2000, 2001). In early attempts by Yousfi et al. (Yousfi et al., 2000, 2001) reported the application of an In_2S_3 buffer layer in CIGS TFSCs for the first time *via* ALE/ALD process, using alternative pulsing of indium acetylacetonate [In(acac)$_3$] and H_2S precursors at 160 °C of deposition temperature. The highest *PCE* of CIGS TFSCs with ALE-grown In_2S_3 buffer layer was 13.5% (with J_{sc} = 30.6 mA/cm^2, V_{oc} = 604 mV and *FF* = 73% at 100 mW/cm^2 without AR coating) for an optimum buffer layer thickness of 30 nm. There was an

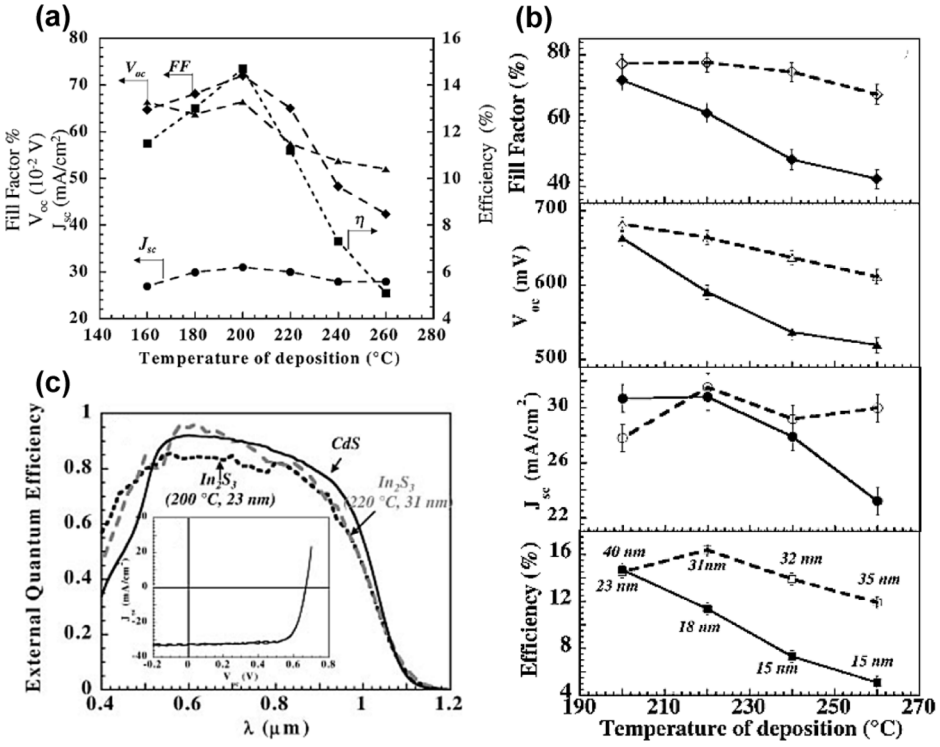

Fig. 11. Influence of the (a) deposition temperature (140–260 °C) and (b) thickness of an In_2S_3 buffer layer on the solar cell parameters of CIGS TFSCs as a function of the temperature of deposition. (c) spectral responses measured under short-circuit conditions on the best cell with an indium sulfide layer deposited at 200 °C (~23 nm) and at 220 °C (~30 nm) compared with a reference cell with CdS buffer layer (Inset shows the *J–V* curves under simulated AM1.5 100 mW/cm^2 illumination performed on the best cell with an In_2S_3 buffer layer deposited at 220 °C). [Reprinted with permission from Naghavi et al. (Naghavi et al., 2003) Copyright 2003, Wiley and Sons].

Table 7
Photovoltaic properties of CIGS cells, with CdS and In_2S_3 buffer layers, with and without Na. [Reprinted with permission from Abou-Ras et al. (Abou-Ras et al., 2005) Copyright 2005, American Institute of Physics].

Buffer, with/without Na	*PCE* [%]	V_{oc} [mV]	*FF* [%]	J_{sc} [mA/cm^2]
CdS, without Na	7.9 ± 0.2	544 ± 2	58 ± 2	25.2 ± 0.5
CdS, with Na	12.6 ± 0.2	649 ± 1	76 ± 2	25.7 ± 0.4
210 °C In_2S_3, without Na	8.7 ± 0.1	603 ± 7	69 ± 1	20.9 ± 0.5
210 °C In_2S_3, with Na	12.6 ± 0.3	686 ± 3	74 ± 2	24.8 ± 0.3

obvious increment in the cell *PCE* as compared with the direct ZnO window without any buffer layer (Table 6). The highest *PCE* obtained with the In_2S_3 buffer layer was also comparable or higher than the standard CdS reference cell possibly due to the formation of a thin interfacial layer during In_2S_3 ALD process that could be resulted in a superficial chemical modification of the CIGS absorber, leading to an improved interface (Guillemoles et al., 2001).

In the further study (Naghavi et al., 2003), a record high *PCE* of 16.4% was achieved with this buffer layers by further extending the deposition temperature window with in the range of 160–260 °C in addition to the more optimization of the buffer layer thickness for two different thicknesses ranges (17 ± 5 and 35 ± 5 nm). A temperature of 200 °C was found to be the optimum with a buffer layer thickness of ~25 nm to obtain the higher *PCE* (Fig. 11a) compared to the previous reported *PCE* of 13.5% at 160 °C (Yousfi et al., 2001). While the variations in the cell parameters were significantly less for the thicker buffer layer, the V_{oc} and *FF* degraded rapidly with increasing deposition temperature for the thinner buffer layer (Fig. 11b). On the other hand, initially J_{sc} of the thicker buffer layer increased with increasing deposition temperature and reached a maximum at 220 °C, after which it was found to decrease. In contrast, the J_{sc} decreased with increasing deposition temperature continuously in the case of the thinner buffer layer. As the cell *PCE* follows the J_{sc}, the highest *PCE* of the cell with an atomic layer chemical vapor deposition (ALCVD)-grown In_2S_3 buffer layer was recorded at a growth temperature of 220 °C and a buffer layer thickness close to 31 nm. The EQE response was found to be higher in the spectral range of 550–900 nm for the In_2S_3 buffer layer compared to the CdS reference cell (Fig. 11c) owing to the larger bandgap of the ALCVD-grown In_2S_3 (2.7–2.8 eV) than CdS (2.5 eV), which helped achieve a higher J_{sc} because of the transparency of buffer layer and better blue response in the EQE spectrum. A preliminary study revealed that the diffusion of Na and Cu into the In_2S_3 buffer layer from CIGS absorber at an elevated deposition temperature without affecting the structural property of the buffer layer, leading to an improved interface quality and junction electrical properties, which probably influenced the TFSCs performances.

A detail investigation on the interface properties of CIGS and ALD-grown In_2S_3 buffer layer junction at a deposition temperature range of 140–240 °C further revealed that at a relatively high temperature (210 °C), some crystal orientation relationships between the {1 1 2) and {1 0 3) planes of the CIGS and In_2S_3, respectively, were observed, while no such relationship was found at 240 °C (Abou-Ras et al., 2005). Furthermore, Cu depletion and emergence of an In-rich CIGS layer at the interface were observed in addition to the Cu and slight Ga diffusion into the In_2S_3 layer, which increased upon increasing the deposition temperature of the buffer layer that resulted in a detrimental effect on the junction due to the formation of an intermediate layer of Cu–In–S compound. In contrast, a large difference in *PCE*s was obtained between the devices with and without Na. Significantly lower *PCE*s were obtained for both the Na-free devices with In_2S_3 as well as CdS buffer layer compared to the devices with Na (Table 7). The devices with Na exhibited better performances as Na helped decrease the diffusion of Cu into the In_2S_3 layer, thereby enhancing the structural, electronic, and optical properties of the buffer layer. The valence band offset for the CIGS/In_2S_3 interface was found to be (–1.2 ± 0.2) eV and (–1.4 ± 0.2) eV for the Na-containing and Na-free layers, respectively (Sterner et al., 2005). The indirect bandgap of ALD-In_2S_3 was found to be close to 2.08 eV, and it did not vary with either the deposition temperature or the buffer layer thickness. By measuring the bandgap of the bulk CIGS absorber (~1.15 eV), the CBO for the CIGS/In_2S_3 interface was determined to be (–0.25 ± 0.2) eV and (–0.45 ± 0.2) eV for the Na-containing and the Na-free CIGS, respectively, which indicate a negative CBO resulting in enhanced interface recombination and thereby poor device performance (Fig. 12a and b).

In 2003, Spiering et al. (Spiering et al., 2003) scaled up the application of ALCVD-grown In_2S_3 buffer layer to a module level (with V_{oc} = 592 mV, *FF* = 62%, and J_{sc} = 29.5 mA/cm^2) with a *PCE* as high as 10.9% for a module area of 30 × 30 cm^2. However, a *PCE* of 14.9% was achieved in a laboratory cell. The effects of deposition temperature as well as the buffer layer thickness on properties of the buffer layer were explored on a mini-module with an area of 5 × 5 cm^2. It was observed that the thickness did not affect the V_{oc} of the cell except a negligible maximum value at a buffer layer thickness of 45 nm (Fig. 13a). However, the overall V_{oc} still remained considerably less than that of the CdS reference cell. On the contrary, the J_{sc} of the laboratory cells consistently decreased with an increase in the buffer layer thickness (Fig. 13b) due to

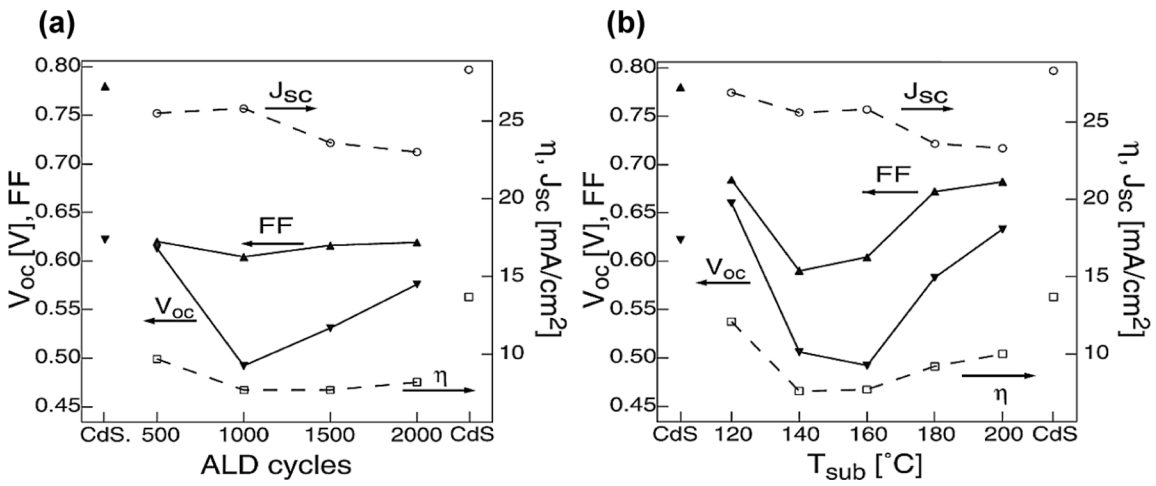

Fig. 12. V_{oc} and *FF* (left-hand axis), and *PCE* and J_{sc} (right-hand axis) as a function of: (a) the number of ALD cycles at a deposition temperature of 160 °C and (b) the ALD substrate temperature (120–200 °C) for 1000 ALD cycles. All values represent the best cells before post-deposition annealing. [Reprinted with permission from Sterner et al. (Sterner et al., 2005) Copyright 2005, John Wiley and Sons].

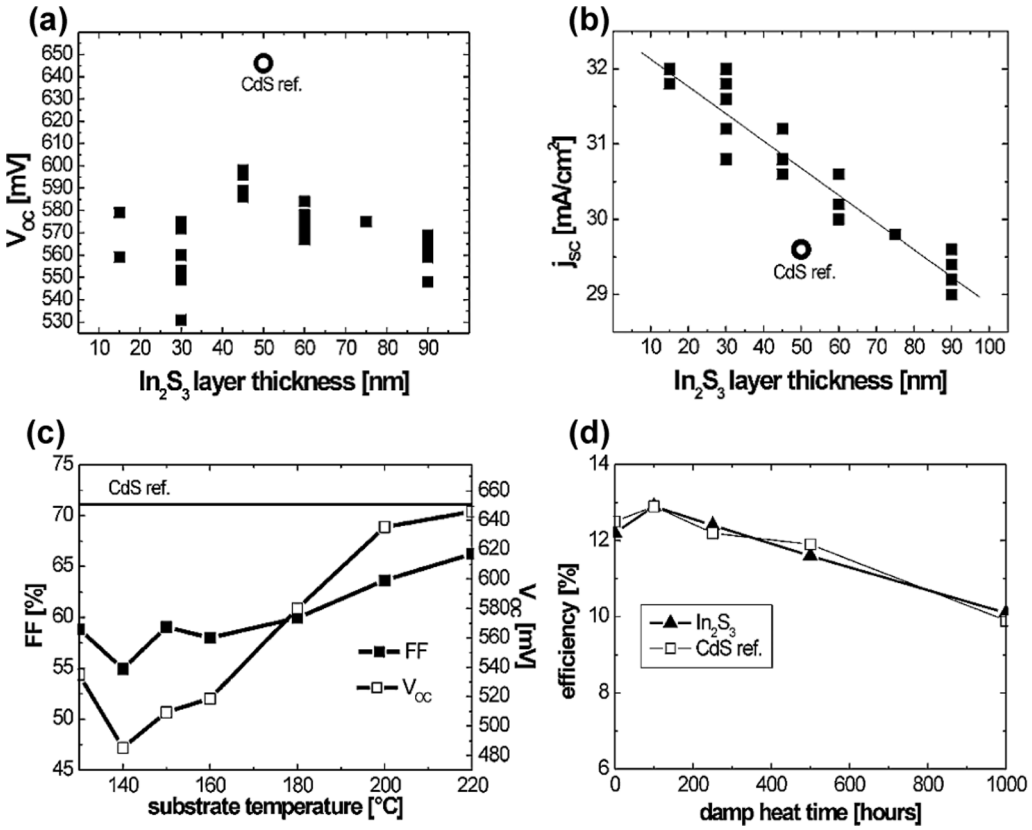

Fig. 13. (a) Open-circuit voltage and (b) current density of as-grown CIGS TFSCs with different In_2S_3 layer thicknesses, T_{dep} = 160 °C. (c) Open-circuit voltage and fill factor of 5 × 5 cm^2 CIGS mini-modules with In_2S_3 buffer layer deposited at different substrate temperatures. (d) The *PCE* of 5 × 5 cm^2 modules during damp heat test. [Reprinted with permission from Spiering et al. (Spiering et al., 2003) Copyright 2003, Elsevier].

the increase in spectral losses as evidenced from the EQE responses. The maximum J_{sc}, much higher than that of the CdS reference cell, obtained at a minimum thickness of 10 nm with an ALCVD process temperature of 160 °C. Furthermore, during the variation of deposition temperature within the range of 130–220 °C, the *FF* and V_{oc} of the module increased significantly upon increasing the substrate temperature and became very much comparable to those of the CdS reference cell (Fig. 13c). Beyond 220 °C, these parameters were found to decrease, resulting in a deteriorated module performance. In addition, a significant improvement in the *FF* and V_{oc} could be obtained by air annealing of the In_2S_3 buffer layer at 200 °C for the laboratory cells when the deposition temperature was 160 °C; however, similar effects were not observed when the ALCVD buffer layer was deposited at 200 °C. The mini-modules with ALCVD-grown In_2S_3 buffer layers exhibited a stable performance over 1000 h of operation at 85% humidity and 85 °C (Fig. 13d) that was comparable with a module with CdS buffer layer where a minimal decrease in the V_{oc} and *FF* was observed while the J_{sc} was almost constant.

A similar higher In_2S_3 deposition temperature or post-deposition annealing effects were also evidenced for the 30 × 30 cm^2 CIGS module, which enabled to obtain a higher *PCE* of ~13% (the output of the module comprising 42 cells: V_{oc} = 27.8 V, *FF* = 72.6%, and I_{sc} = 0.457 A) when both the In_2S_3 buffer as well as i-ZnO layer deposited at an higher temperature (Spiering et al., 2004) owing to the temperature-dependent diffusion (both deposition and post-annealing temperatures) of Cu and Na at the CIGS/In_2S_3 interface. The temperature-dependent cell performance (Fig. 14a) indicated that the *PCE* could be significantly increased by a post-annealing treatment in air in addition to an elevated process temperature. It is apparent from this discussion that the ALD-grown In_2S_3 buffer layer has been studied extensively; it can be established that In_2S_3 is a potential alternative to CdS, even at the scale of a 30 × 30 cm^2 module with a high *PCE* of ~13% as reported. However, only a few reports on long-term stability of such modules with ALD-grown In_2S_3 buffer layers are available. Spiering et al. (Spiering et al., 2005) investigated the stability of such Cd-free CIGS modules; their work truly helped in judging the potential of ALD-grown In_2S_3 buffer layers for implementation in industries. The indoor long-term stability of such modules under damp heat conditions and by thermal cycling, the In_2S_3 buffer layers showed a very good stability comparable with that of the CBD-CdS reference module. The outdoor testing results over 16 months were also promising. Thus, it demonstrated the feasibility of a Cd-free high-efficiency CIGS TFSC with ALD-grown buffer layer. Furthermore, the light soaking revealed negligible effect on ALD-grown In_2S_3 buffer layers, which is quite contradictory to the tendency exhibited by other ALD-grown buffer layers.

Apart from the aforementioned studies on In_2S_3 buffer layer, recently, Bugot et al. reported an indium oxysulfide [$In_2(O,S)_3$] buffer layer for CIGS TFSCs with the combined process of thermal ALD and plasma-enhanced ALD (PEALD) (Bugot et al., 2018) using the same precursors for sourcing In and S (Yousfi et al., 2000), while an O_2/Ar plasma was used as source of oxygen for the deposition of $In_2(O,S)_3$ thin films at a substrate temperature of 160 °C. In addition, a precise control over the film properties and stoichiometry by varying the ALD super-cycles led to fine-tuning of the optical bandgap in the range of 2.2–3.3

Table 8
J–V parameters of the devices with CBD-CdS and ALD-grown $In_2(O,S)_3$ buffer layers deposited on CIGS absorber.

Buffer layer	V_{oc} [mV]	J_{sc} (EQE) [mA/cm^2]	*FF* [%]	*PCE* [%]
CIGS/CdS	640	26.9	76	13.2
CIGS/$In_2(S,O)_3$	650	26.7	69	11.9

eV, higher than the pristine In_2S_3 buffer layer, which was an added advantage of this ternary O-incorporated $In_2(O,S)_3$ buffer layer. Furthermore, the $In_2(O,S)_3$ buffer layer of 16 nm in thickness was implemented on CIGS absorber by the modified deposition parameters, and the *J–V* characteristics under illumination were determined, as shown in Fig. 14b. The device performance was comparatively inferior compared with a reference device with CdS buffer layer (Table 8). However, the obtained V_{oc} value was slightly higher for the $In_2(O,S)_3$ buffer layer.

3.7. Other ALD-grown buffer layers

This section includes relatively less studied materials which comprise both the Zn as well as In-based compound (zinc indium sulphide; ZnInS), in addition to the pristine TiO_2 and Zn-Ti-based compound buffer layer (ZnTiO). To the best of our knowledge, there are only one report available for each of these buffer material and among them ZnTiO produced promising outputs in view of device performance when compared with the reference device with CdS buffer layer as well as other most efficient ALD buffer layer discussed in this article.

The feasibility of using ZnInS as a buffer layer in CIGS TFSCs was reported by Genevee et al. (Genevée et al., 2015). The DEZ, indium acetylacetonate [$(In(CH_3COCHCOCH_3)_3$; In(acac)$_3$], and H_2S were used as the precursors for the deposition of ZnInS by ALD (Genevée et al., 2011, 2013) at 180, 200, and 220 °C with the In/(In + Zn) ratio ranging from pure ZnS to pure In_2S_3. The cell with a pure In_2S_3 buffer layer exhibited *J–V* characteristics similar to those of a CdS reference cell.

Table 9
V_{oc}, J_{sc}, *FF*, and *PCE* of the best CIGS/TiO_2 solar cell as well as the CIGS/CdS reference solar cell alongside with stability measurements of a CIGS/TiO_2 (15 nm TiO_2 deposited at 120 °C) and CIGS/CdS solar cell re-measured after 9 months and under light soaking. [Reprinted with permission from Hsu et al. (Hsu et al., 2015) Copyright 2015, Springer Nature].

	Configuration	V_{oc} [mV]	J_{sc} [mA/cm^2]	*FF* [%]	*PCE* [%]
Best	CdS/CIGS	416	36.9	61.4	9.5
	TiO_2/CIGS	426	38.9	59.6	9.9
Stability test, first measured	CdS/CIGS	401	38.2	55.8	8.5
	TiO_2/CIGS	404	39.8	56.4	9.1
After 9 months	CdS/CIGS	396	36.2	52.5	7.5
	TiO_2/CIGS	399	40.0	50.7	8.1
After 9 months + light soak	CdS/CIGS	395	36.1	53.2	7.6
	TiO_2/CIGS	404	40.2	56.5	9.2

Individual cells are scribed into areas of 3.5 × 3.5 mm^2, resulting in an active area of 10.5 mm^2.

Though the J_{sc} was almost similar to that of the CdS cell, the V_{oc} and *FF* were lower. This can be due to the negative CBO at the CIGS/buffer interface, which influences the interface recombination (Minemoto et al., 2001; Sterner et al., 2005). With an increasing In/(In + Zn) ratio, an In-rich buffer layer showed a better performance though the cell parameters were lower than those of a CdS reference cell. A cell with a ZnInS buffer layer grown with an In/(In + Zn) ratio of 28% resulted in a J_{sc} similar to a cell with an In-rich buffer layer, along with a V_{oc} that is higher than that of a CdS reference cell. However, the *PCE* of the cell was

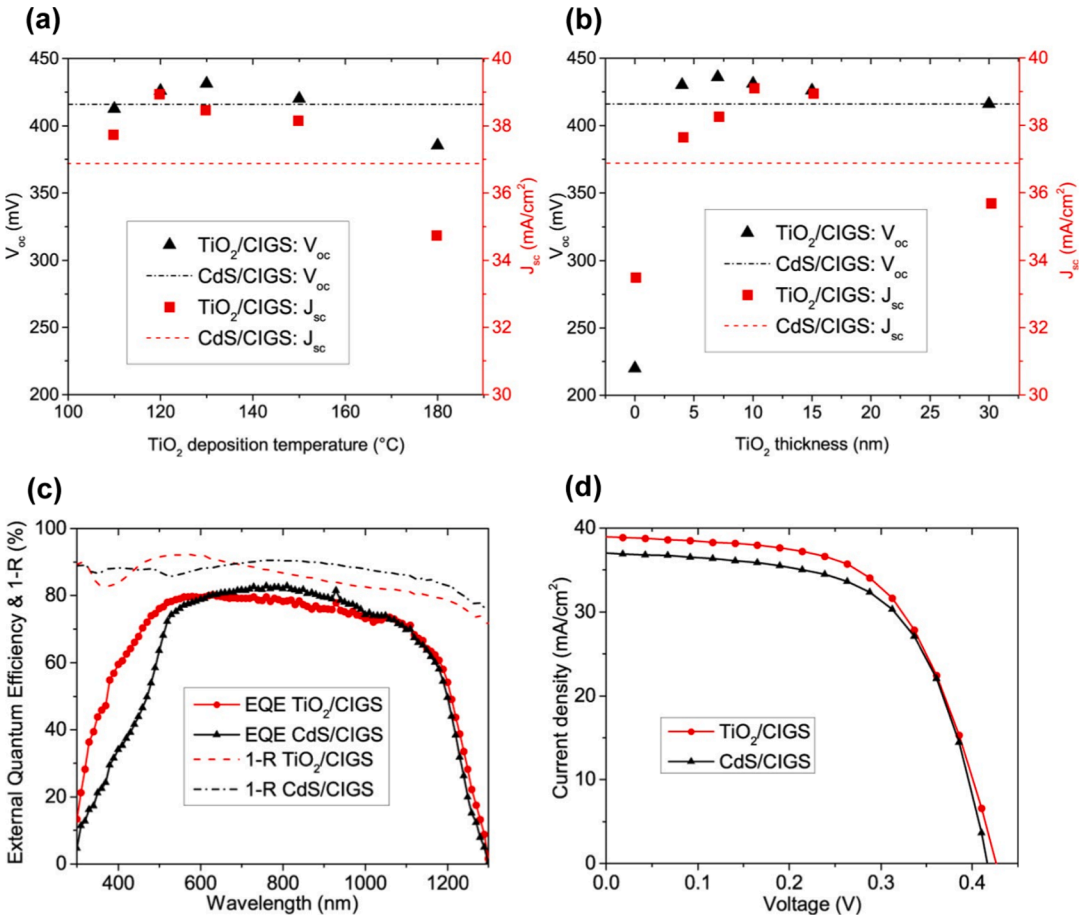

Fig. 15. (a) Dependence of V_{oc} and J_{sc} on TiO_2 deposition temperature (at fixed TiO_2 thickness of 15 nm), (b) dependence on TiO_2 thickness (at fixed deposition temperature of 120 °C). The V_{oc} and J_{sc} of the CdS reference cell are given as dashed lines. (c) EQE and 1-Reflectance curves of the CIGS/TiO_2 and CIGS/CdS solar cells, (d) *J–V* curves of CIGS/TiO_2 and CIGS/CdS solar cells corresponding to the EQE data shown in (c). [Reprinted with permission from Hsu et al. (Hsu et al., 2015) Copyright 2015, Springer Nature].

limited to 6.6% by a poor *FF*. Meanwhile, a cell with a Zn-rich buffer layer fared poorly due to the interface recombination caused by the formation of a large spike at the CIGS/ZnInS interface. The EQE response of a ZnInS-based cell was equivalent to that of a pure In_2S_3-based cell in the longer wavelength range. An improved response was observed in the lower wavelength range due to the wide bandgap of the ZnS buffer layer as compared to the pure In_2S_3 and CdS buffer layers. The lower response of ZnS throughout the wavelength range was attributed to the interface recombination. The performance of the ZnInS-based cells with an In/(In + Zn) ratio of 28% improved with a decrease in the ALD deposition temperature, which indicates a reduction in the defect states at the buffer/window layer interface. Thus, it was proved that ZnInS is a potential alternative to CdS in CIGS TFSCs.

The only report on ALD-grown alternative buffer layer that neither involve Zn nor In, is TiO_2, deposited by titanium isopropoxide [$Ti[OCH(CH_3)_2]_4$] and H_2O as the ALD precursors, showed a higher *PCE* as compared to previously mentioned ZnInS buffer layer. Hsu et al. achieved a higher *PCE* of 9.9% using this *n-type* amorphous ALD-grown TiO_2 buffer layer compared to 9.5% of reference device with CdS buffer layer on an active cell area (*S*) of 10.5 mm^2 (Hsu et al., 2015). Both the deposition temperature and thickness of the buffer layer were varied to maximize the obtained *PCE*. An increase in the deposition temperature from 110 to 130 °C resulted in a certain increase in the V_{oc} up to 431 mV (416 mV for CdS reference cell) with a maximum J_{sc} of 38.9 mA/cm^2 (at 120 °C; where 36.9 mA/cm^2 for reference cell) (Fig. 15a). According to the author, the enhancement in V_{oc} was possibly due to the reduction in interface recombination owing to the formation of an inverted surface at CIGS/TiO_2 junction as a consequence of the elemental interdiffusion. In contrast, a further increase in deposition temperature to 180 °C led to a continuous drop in both the V_{oc} as well as J_{sc} (Fig. 15a) might be due to the phase transformation of TiO_2 from amorphous to nanocrystalline, which resulted in an increase in roughness owing to the small crystallites formation. On the other hand, a substantial loss in J_{sc} was revealed beyond the optimized thickness (10–15 nm) of ALD-grown TiO_2 buffer layer (Fig. 15b) owing to the residual light absorption. The photocurrent gain in the UV part of the spectrum could be attributed to the wider bandgap of TiO_2 (3.4 eV) than CdS, which led to a higher J_{sc} of the CIGS TFSC with this alternative buffer layer because of lower parasitic absorption loss. However, the *FF* of the device with TiO_2 (59.6%) buffer layer was slightly lower than the reference CdS (61.4%) cell. This was probably due to the higher R_s value of the CIGS/TiO_2 junction typically for the highly resistive TiO_2 thin film, which could be reduced further by elemental doping in the TiO_2 layer. Fig. 15c and d show the EQE (with reflectance) measurements and *J–V* characteristics of the CIGS-based TFSCs, respectively, with ALD-grown TiO_2 and CBD-CdS buffer layer, which clearly depict a superior device performance using ALD-grown alternative buffer layer.

Finally, this study revealed a considerably more stable CIGS TFSC using TiO_2 buffer layer with a slight improvement in *PCE* after the 20 min light soaking after a period of nine months. Table 9 shows the highest *PCE* and stability test achieved in this study. Therefore, further research on ALD-grown TiO_2 based buffer layer is very much expected to enhance the cell performance beyond this study.

Recently Hwang et al. (Hwang et al., 2018) published the pioneer report on ALD-deposited ZnTiO buffer layer for CIGS TFSCs using DEZ and tetrakis diethylamino titanium [$Ti[(C_2H_5)_2N]_4$] as metal precursors and H_2O as reactant at 150 °C with different ZnO:TiO_2 ALD cycle ratios. A detailed study of the properties of an ALD-ZnTiO film revealed an increase in resistivity and a decrease in carrier concentration of the film with a change in Zn:Ti cycle ratio (from 7:1 to 3:1). On the other hand, an increase in bandgap was observed within a range of 3.21–3.62 eV for a ZnTiO film with a gradual loss in crystallinity owing to the increase in Ti content. ZnTiO buffer layers with an optimized cycle ratio of 4:1 exhibited a negative CBO (−0.11 eV) at the CIGS/ZnTiO interface as shown in Fig. 16a. The achieved *PCE* of a CIGS/ZnTiO device obtained with a cycle ratio of 4:1 was very low (~0.16%) compared with a reference CIGS/CdS device. However, a significant improvement was observed after a wet pre-treatment of CIGS absorber with NH_4OH, Cd^{+2}, and H_2O, which etched the Na-compounds from the CIGS surface, thereby leading to a *PCE* that is 80% of that of the reference CIGS/CdS

Table 10
Photovoltaic parameters of CIGS solar cells with ZnTiO buffer layer. [Reprinted with permission from Hwang et al. (Hwang et al., 2018) Copyright 2018, American Institute of Physics]

With/without wet pretreatment	V_{oc} [V]	*FF* [%]	R_{sh} [Ω-cm^2]	R_s [Ω-cm^2]	J_{sc} [mA/cm^2]	*PCE* [%]
CIGS/CdS	0.63	70.42	24158.30	5.41	34.37	15.44
CIGS(Bare)/ ZnTiO	0.04	25.06	6.50	6.84	15.42	0.16
CIGS(NH_4OH)/ ZnTiO	0.58	60.60	895.08	9.14	29.82	10.56
CIGS(H_2O)/ ZnTiO	0.58	59.18	699.28	9.97	31.76	10.99
CIGS(Cd)/ZnTiO	0.61	64.07	926.25	7.888	31.90	12.46

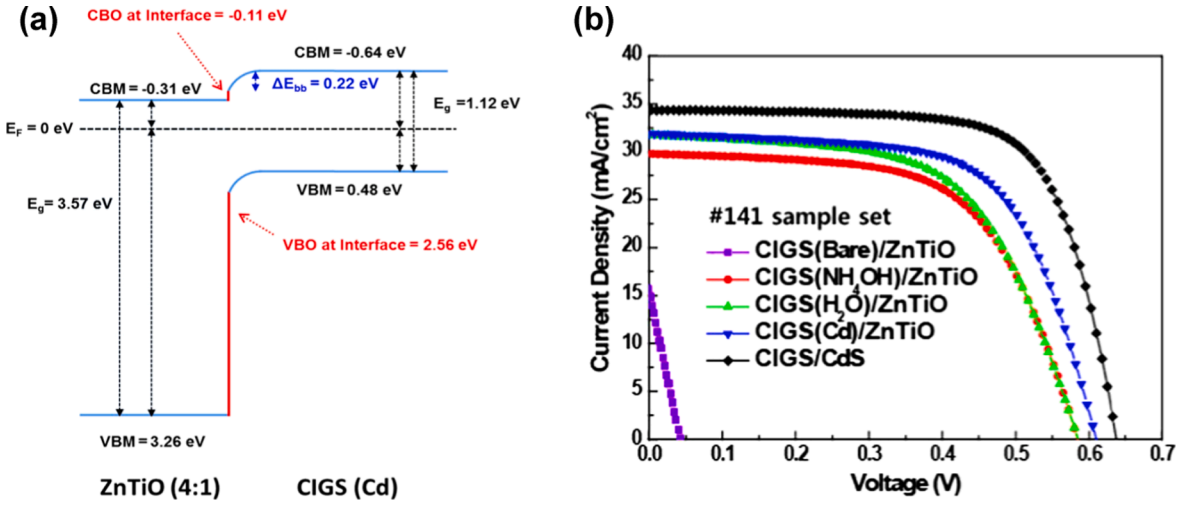

Fig. 16. (a) Energy band diagram of the CIGS(Cd)/ZnTiO, and (b) A representative set of *J–V* characteristics of various wet chemical-treated CIGS TFSCs with ZnTiO buffer layer and of CdS reference cell [Reprinted with permission from Hwang et al. (Hwang et al., 2018) Copyright 2018, American Institute of Physics].

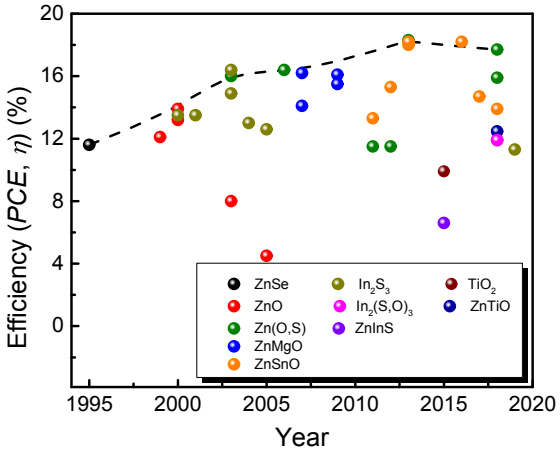

Fig. 17. A graphical representation of the *PCE* improvement for CIGS-based TFSCs with different ALD-grown Cd-free alternative buffer layers. (Abou-Ras et al., 2005; Agbenyeke et al., 2018; Bugot et al., 2018; Chaisitsak et al., 1999, 2000; Genevée et al., 2015; Guillemoles et al., 2001; Hsu et al., 2015; Hultqvist et al., 2009, 2011a, 2011b, 2012; Hwang et al., 2018; Illiberi et al., 2018; Kobayashi et al., 2013; Larsson et al., 2018; Le Tulzo et al., 2019; Lindahl et al., 2013a, 2013b, 2016; Malm et al., 2005; Naghavi et al., 2003; Nakashima et al., 2012; Ohtake et al., 1995; Pettersson et al., 2009; Platzer-Björkman et al., 2003b, 2003c, 2006, 2007; Salomé et al., 2017; Shimizu et al., 2000; Spiering et al., 2003, 2004, 2005; Sterner et al., 2005; Törndahl et al., 2007, 2009, Yousfi et al., 2000, 2001).

Table 11
Highest *PCE*s that achieved for CIGS-based TFSCs till date with ALD-grown Cd-free alternative buffer layers in comparison with their CdS reference cells (if available).

ALD-grown buffer layer	Buffer layer thickness [nm]	Highest *PCE* [%]	CdS reference *PCE* [%]	Ref.
ZnSe	10	11.6	N/A	(Ohtake et al., 1995)
ZnO	70	13.9	N/A	(Chaisitsak et al., 2000)
Zn(O,S)	50	18.3	N/A	(Kobayashi et al., 2013)
ZnMgO	150	16.2	15.4	(Platzer-Björkman et al., 2007)
ZnSnO	13 ± 5	18.2	18.6	(Lindahl et al., 2013b)
	40 ± 5	18.3	17.9	(Lindahl et al., 2016)
In_2S_3	30	16.4	N/A	(Naghavi et al., 2003)
$In_2(S,O)_3$	16	11.9	13.2	(Bugot et al., 2018)
ZnInS	15	11.2	12.3	(Genevée et al., 2015)
TiO_2	10	9.9	9.5	(Hsu et al., 2015)
ZnTiO	60	12.46	15.44	(Hwang et al., 2018)

TFSC as shown in Fig. 16b and Table 10.

4. Current challenges and future scopes

This review article exhibits the significant applications and success of ALD-grown buffer layer as an efficient alternative to CdS in CIGS-based TFSCs in accordance with the current trend that reflects the slowest increment or rather saturation in *PCE* compared to its theoretical limit of 33.5% (Yin et al., 2015). While the *PCE* for CIGS-based TFSCs with state-of-the-art CdS buffer layer just reached above 20% (highest *PCE* reported so far for a laboratory-based CIGS cell: ~23%) in past few years (Green et al., 2018; Jackson et al., 2016; Menner et al., 2017), a similar trend of a saturated *PCE* with Cd-free ALD-grown buffer layer could be realized for CIGS TFSCs (Fig. 17). In the case of ALD-grown buffer layer, the *PCE* has not reached much beyond 18% (highest: ~18.3%) for CIGS-based TFSCs; however, several individual reports achieved the *PCE*s either very close or even higher compared to the reference cell with CdS buffer layer, as shown in Table 11. Here, one should also note that a combination of ALD-CBD double buffer layer recently delivered a highest PCE of >23% as discussed in detail later in this section. From the table, it could be realized that an improvement in the CIGS properties would automatically result in higher *PCE* with ALD-grown buffer layer.

Therefore, in this section, we identify several challenges and possibilities for further enhancement of *PCE* of CIGS-based TFSCs. Apart from the improvements in buffer layer attributed to ALD, the improvements in the opto-electronic properties of CIGS absorber itself such as an increased light absorption or a minimized bulk recombination can be realized through necessary approaches to increase the overall performance of a TFSC. Similarly, there are other properties of CIGS absorber layer such as stoichiometry, surface morphology, grain size, defect states, and interfaces with buffer and the Mo back contact that affect the performance of a TFSC. The bandgap of the CIGS absorber can be tuned with stoichiometry, to maximize the collection efficiency of the photo-generated carriers (Ramanujam and Singh, 2017). In this regard, a graded-type bandgap composition was reported by varying the Ga concentration along the depth of the CIGS layer, which improved the electronic properties and thereby the V_{oc}, J_{sc}, and *PCE* of the TFSCs (Contreras et al., 1994; Yoshiaki et al., 2014, 2012). However, it has been observed that the device performance deteriorates for a high Ga content that increases the defect density thereby reducing the quality of CIGS absorber layer (Larsson et al., 2017; Pettersson et al., 2013). Therefore, a proper and carefully controlled optimization of Ga concentration is needed to achieve a high-*PCE* CIGS-based TFSC with a graded bandgap. Furthermore, the quality of CIGS absorber can also be improved through different approaches like Na-diffusion from SLG as mentioned by Ramanujam et al. in their review on CIGS-based TFSCs (Ramanujam and Singh, 2017). In general, the influence of a small amount of light/heavy alkali metals like Li, Na, K, Cs, Rb *etc*. opened up a different pathway to improve the CIGS absorber quality, CdS buffer layer coverage/thickness control, and thereby an effective influence on the performance of the devices (Asaduzzaman et al., 2016; Chirilă et al., 2013; Ishizuka and Fons, 2020; Kodalle et al., 2019; Mufti et al., 2020). However, similar research is still limited when ALD-grown buffer layer is investigated for CIGS-based TFSCs. Therefore, PDT of the CIGS surface with NaF, KF, RbF *etc*. might offer another plausible way for future study while exploring the ALD-grown buffer layer as an alternative to CBD-CdS. On the other hand, the defect density can be reduced by using a surface passivation layer on both sides of CIGS absorber *i.e*. Mo/CIGS and CIGS/buffer layer interfaces. This reduces the recombination losses, thereby resulting in higher J_{sc} and probably higher V_{oc} as well. Interestingly, ALD shall also play a critical role in depositing these interfacial passivation layers such as Al_2O_3, in addition to buffer layer. However, there are few reports till date in this direction, and more research with other suitable materials could help realize a better *PCE* for CIGS-based TFSCs (Kotipalli et al., 2015; Vermang et al., 2014, 2013).

In contrast, according to a recent review article by Ochoa et al., the material quality of CIGS is about to reach an extreme limit delivering the highest possible efficiency of a single-junction cell (Ochoa et al., 2020). Therefore, they have recommended some paradigm shift in the device architecture associated with CIGS-based TFSC technology which can only boost the *PCE* further. Some of these approaches identified by the authors include a non-graded/thinner absorber, selective front and rear contact, re-absorbing the photons generated by radiative recombination inside CIGS layer (photon recycling) *etc*. In this regard, it can be noted

that several feasible strategies have already been implemented successfully for III–V PV technology, like efficient back reflectors with a high reflectance as well as good ohmic contact, use of metal and/or oxide layers instead of only TCO, charge selective contacts, high and controlled elemental doping concentration, enhancement of non-radiative lifetimes *etc*., to resolve the issues associated to the inferior device performance (Bauhuis et al., 2009; Bissig et al., 2018; Ochoa et al., 2020). Though most of the issues are also similar in CIGS-based TFSCs and implementation of such strategies might be the plausible way for the performance enhancement of the devices; however, till now, it is a great challenge for the CIGS PV community to apply these methodologies during the device fabrication, while a direct transfer of this methods may not be possible for CIGS-based TFSCs in reality.

Beside pure Se-based CIGS absorber, the S incorporated *p-type* Cu(In, Ga)(S,Se)$_2$ (CIGSSe), a CIGS-type absorber material, has also been drawn a significant attention as another promising and favorable absorber for TFSCs that reveals an average *PCE* of >20% for Cd-based/Cd-free TFSCs in past few years by utilizing the graded bandgap concept (Chantana et al., 2019, 2020b; Feurer et al., 2017; Kato et al., 2019; Kong Fai et al., 2017; Naghavi et al., 2010; Takuya, 2017). In a most recent report, Nakamura et al. (Nakamura et al., 2019) have achieved a record *PCE* of 23.35% for Cd-free CIGSSe-based TFSCs developed by Solar Frontier. Here, the metal precursor sputtering followed by the subsequent selenization and sulfurization (SAS) processes are used to obtain a stack of Cu–In–Ga and finally CIGSSe absorber, respectively, instead of a conventional co-evaporation used for CIGS deposition. Along with controlled composition of Cu–In–Ga, the subsequent SAS processes form the S-rich layer at CIGSSe/buffer interface that results in a hole blocking layer by lowering the valence band, while a Ga gradient is found at the back Mo contact interface that pushes the conduction band up. Therefore, this gradient in bandgap profile usually prevents electron–hole recombination at both the front as well as back interfaces and enables carrier transport and collection, which leads to a better performance of the TFSCs (Kamada et al., 2016; Khatri et al., 2015; Nakamura et al., 2019; Takuya, 2017). Additionally, a major influence of PDT on the absorber material with alkali elements such as K or Cs is also found to be beneficial for further performance enhancement of the CIGSSe-based TFSCs (Chantana et al., 2020a; Kato et al., 2019; Kong Fai et al., 2017; Nakamura et al., 2019). Nevertheless, Cd-free ALD-grown single buffer layer like Zn(O,S) has been applied for this CIGS-type CIGSSe-based TFSCs and even for mini-module also, which reveals a comparable and even superior performances (highest *PCE* is ~20%) compared to that of the reference CBD-grown CdS buffer layer (Bin Mo et al., 2019; Kobayashi et al., 2016; Merdes et al., 2014, 2015). In contrast, the application of Cd-free double buffer layers for CIGSSe TFSCs by Solar Frontier, in which the second buffer layer is usually ZnMgO deposited by ALD in combination with CBD-grown Zn(O,S,OH) as first buffer layer, shows higher *PCE*s compared to the devices with only CdS buffer layer or a second buffer layer grown by other deposition processes, *e.g.*, metal organic chemical vapor deposited (MOCVD) ZnO (Kamada et al., 2016; Kong Fai et al., 2017; Nakamura et al., 2019). In this context, it should be noted that the application of these CBD and ALD-grown double buffer layers reveals the recently reported record *PCE* of 23.35% for the CIGSSe-based TFSCs (Nakamura et al., 2019) with respect to their previously achieved highest *PCE* of 22.92% with only CBD-CdS buffer layer (Kato et al., 2019). The performance improvement is possibly due to the reduction in recombination at the absorber/buffer interface for the application of double buffer layers. Thus, these investigations open a new path for further improvement in the device performances in future and also corroborate the superiority of ALD technique to deposit several buffer layers.

In addition, as a quaternary material, it is also difficult to deposit CIGS absorber with uniform thickness and composition on large-area substrates, which directly affects its electronic and optical properties that are critical to achieve a high *PCE*, especially for large-area TFSCs. It is indicative of the challenges in scaling up the CIGS TFSCs for an industry level production from a lab-scale process with a comparable *PCE*. The commercial module *PCE* is still way below the lab-scale *PCE* due to the inhomogeneous growth of CIGS absorber layer over a large area, which can be improved using an in-line growth process for the TFSC modules. Similar issues of uniformity and homogeneity are also very much associated with the conventional CdS buffer layer owing to its wet chemical synthesis. Therefore, the vacuum-based ALD has a great prospect for the deposition of buffer layer instead of CBD-CdS buffer layer in addition to the absorber and window layer, which solves both the issue of toxicity associated with Cd as well as the issue of substrate handling between different fabrication tools. In this context, a recent investigation by Tulzo et al. (Le Tulzo et al., 2019) reports the application of ALD process for the fabrication of a complete structure TFSC with a film stack of glass/Mo/CIS/In_2S_3/ZnO/ZnO:Al (considered as "nearly CIGS-type TFSC"), where only ALD has been used to deposit all the layers, i.e., from the absorber to the window layer. Primarily, a *PCE* of 11.3% has been achieved with an optimized 10-nm-thick ALD-grown In_2S_3 buffer layer and ALD-grown ZnO/ZnO:Al window layer deposited at 200 °C for a 2 μm-thick co-evaporated CIGS absorber, which is comparable with the *PCE* of 13.2% with CBD-CdS buffer layer and PVD (sputtering)-grown window layers. Though the performance of the all-ALD-grown CIS-based TFSCs is very low due to several reasons, especially owing to the lack of optimization in addition to the thinner absorber (60 nm) and buffer layer (10 nm), properties (lower electrical conductivity) of window layer *etc*., but this approach shows a promising way toward the development of ALD-grown TFSCs, which encourage for the further challenges to obtain the TFSCs with an extremely thin absorber on large and 3D-nanostructured substrates by using exclusive thin film deposition capabilities of the ALD technique.

In addition, another recent article by Stamford et al. investigates the life-cycle environmental impacts (like global warming potential in terms of g-CO_2 eq./kWh, ecotoxicity, waste at the end-of-cycle use *etc*.) of a state-of-the-art CIGS PV system installed in UK and Spain and the results are not only discussed in light of other thin-film based PV technologies (like a-Si and CdTe) but also confirms a feasibility of ALD-grown Zn(O,S) buffer layer to replace the conventional CdS layer (Stamford and Azapagic, 2019). The study further finds that the overall environmental impacts becomes only 0.01% (across the life cycle) with ALD-grown Zn

Table 12
Impacts of chemical bath deposition (CBD) and atomic layer deposition (ALD) per square metre of coated substrate. [Reprinted with permission from Stamford et al. (Stamford and Azapagic, 2019) Copyright 2019, Elsevier].

Impact (per m^2 of coated substrate)	CBD of CdS[a]	ALD of Zn(O, S)
Climate change, exc. biogenic carbon [kg CO_2 eq.]	0.582	0.302
Fine particulate matter formation [g PM2.5 eq.]	0.491	0.182
Fossil depletion [kg oil eq.]	0.213	0.0948
Freshwater consumption [m^3]	0.991	0.804
Freshwater ecotoxicity [g 1,4 DB[b] eq.]	28.1	1.07
Freshwater eutrophication [g P eq.]	0.360	0.286
Human toxicity, cancer [g 1,4-DB eq.]	28.8	19.3
Human toxicity, non-cancer [kg 1,4-DB eq.]	3.66	0.327
Ionizing radiation [mBq C-60 eq. to air]	100.2	69.2
Land use [annual crop eq.·y]	5.75×10^{-3}	4.59×10^{-3}
Marine ecotoxicity [g 1,4-DB eq.]	35.2	1.74
Marine eutrophication [mg N eq.]	30.3	19.6
Metal depletion [g Cu eq.]	1.68	4.46
Photochemical ozone formation, ecosystems [g NO_x eq.]	1.06	0.419
Photochemical ozone formation, human health [g NO_x eq.]	1.04	0.401
Stratospheric ozone depletion [mg CFC-11 eq.]	0.314	0.165
Terrestrial acidification [g SO_2 eq.]	1.33	0.501
Terrestrial ecotoxicity [kg 1,4-DB eq.]	1.52	0.592

[a] Includes an estimate of electricity consumption based on electricity used in the ALD process.
[b] DB: dichlorobenzene.

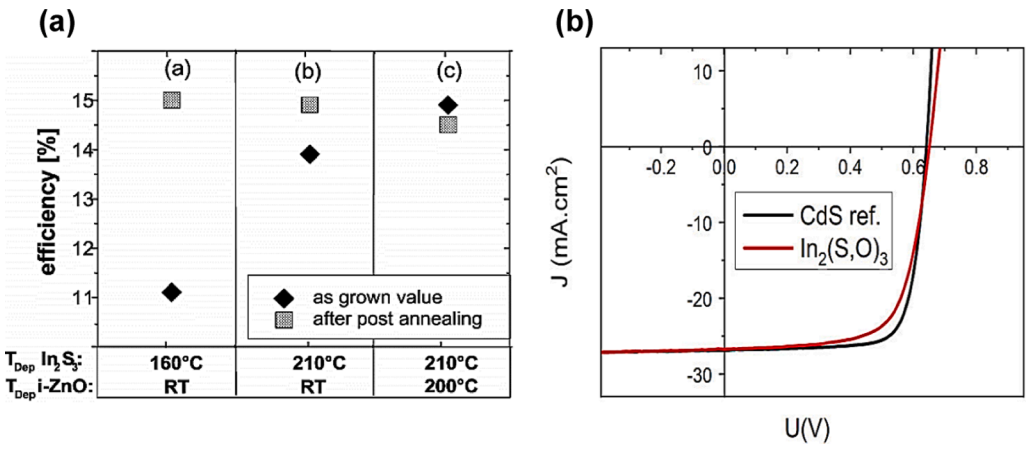

Fig. 14. (a) Efficiencies of Cd-free laboratory cells (S = 0.5 cm^2) under varying process conditions of the In_2S_3 and i-ZnO depositions. The PCE was determined before and after a post-annealing in air at 200 °C for 1 h. [Reprinted with permission from Spiering et al. (Spiering et al., 2004) Copyright 2004, Elsevier]; (b) *J–V* curves of borosilicate glass/Mo/CIGS/buffer layer/ZnO/ZnO:Al solar devices under illumination with buffer layers: CdS, $In_2(O,S)_3$. [Reprinted with permission from Bugot et al. (Bugot et al., 2018) Copyright 2018, American Vacuum Society].

(O,S) buffer layer compared to 0.5% of CdS. Table 12 compares several environmental impacts of CdS and ALD-Zn(O,S) on a life-cycle basic.

Therefore, the authors recommend that highly toxic Cd could be avoided by PV manufacturers as ALD-grown buffer layer would not degrade the performance but will have a positive effect when considered with overall environmental impacts. The work shows true promise towards applying ALD commercially to CIGS PV system that could be installed on ground. Similar systematic studies with other ALD-grown buffer layers which are established to a good extent (like (Zn,Mg)O, In_2S_3 *etc.*) would also be appreciated for a CIGS module to establish the credibility of ALD towards its commercial applications.

Nevertheless, there are practical issues in accommodating the cells (or module) of larger size in the ALD reactors of larger capacity to enable high throughput. In this regard, there are already several approaches taken to handle large-scale processing *via* ALD (Delft et al., 2012; Sinha et al., 2018a). Despite, the current research seems to concentrate more to increase the existing *PCE* of a lab-based solar cell first. Scaling up for ALD-grown buffer layer with a comparable *PCE* with that of CBD-CdS based TFSC might not show an economic feasibility at this moment. A step-wise effort to increase the active cell area while keeping the *PCE* intact would be a possible solution in this regard. ALD is now rapidly becoming a more common and popular technique to be used in the renewable energy field in the research community. Therefore, we hope that this film deposition technique will draw enough attention from the industry involving similar research and development which can facilitate the production of CIGS modules based on ALD-grown buffer layer at a commercial scale.

Finally, TFSCs on flexible substrates have recently attracted considerable attention due to their possible implementation in integrated photovoltaics that includes the vehicle-integrated photovoltaic (VIPV), building-integrated photovoltaic (BIPV), wearable solar cells, *etc.* (Chirilă et al., 2011; Kessler et al., 2005; Otte et al., 2006; Peng et al., 2014; Shah et al., 2004; Yoon et al., 2011). In addition to several advanced applications of these flexible TFSCs, reduction in production cost can also be possible using a roll-to-roll fabrication process. Even though significant progress has already been made to realize high-*PCE* CIGS TFSCs on different flexible substrates, most of them are mainly restricted to lab-scale device fabrication and need further research and development for a large-scale industrial production. Apart from the challenges related in achieving a good quality CIGS absorber layer, which usually needs high temperature growth process, the incompatibility of the deposition of buffer layer particularly for CBD-CdS is a critical factor to be addressed as it restricts realizing a large-area high-*PCE* TFSC on a flexible substrate. Nevertheless, most of the ALD-grown buffer layers that yielded best performances in CIGS-TFSCs could be effectively deposited well within the temperature limit (~up to 250 °C) that the polymer-based flexible substrates can withstand. Moreover, the ALD was successfully demonstrated on flexible substrates.

It is clear that ALD is more advantageous as one of the most favorable techniques than CBD in respect of compatibility among others owing to the vacuum process for growth of CIGS, and therefore has enough potential to replace the toxic CdS as a conventional buffer layer for large scale production. The scaled-up ALD reactors with improved technologies should make this a reality in near future. In addition, the most recently introduced ALD-grown Zn-based ternary buffer layer (ZnTiO) needs to be explored for further optimization to enhance *PCE* to a level higher than the current highest value using ALD-grown buffer layer (Hwang et al., 2018). Similarly, there are several scopes to study newer ALD-grown Zn-based ternary and other binary/ternary materials with excellent opto-electronic properties and a better band alignment with CIGS. Other possible combination of Zn-based material with new transition metal (TM, Zn-TM-O/S) might help tune the opto-electronic properties better than the existing materials. In addition, Ta_2O_5, InSe, ZnInSe or SnOS might also be attempted as new ALD-grown alternative buffer layers. In this regard, a theoretical study of several combinations of such materials may help target newer buffer materials prior to performing experiments. Furthermore, not only a single buffer layer but also an application of two separate ALD-grown buffer layers with different bandgaps might also facilitate the photogenerated carrier's separation and collection by providing a superior band alignment between CIGS/buffer layer interface and window layer. In any case, a continuous research on ALD is very much expected to identify new materials that will take their application as a buffer layer in CIGS TFSCs to the next level. Furthermore, the drawbacks with the existing ALD-grown buffer layers (Zn(O,S) and ZnMgO) that exhibited the highest *PCE* should be resolved. In spite of the excellent uniformity offered by ALD, the ALD-Zn(O,S) on CIGS suffered considerably from non-uniformity which would eventually degrade the performance of the cell (Hultqvist et al., 2011b). On the other hand, ZnMgO was observed to degrade with light exposure that converted it to a metastable state (Pettersson et al., 2009). Considering further its promising future, ALD-grown buffer layers should also be tried in CIGS-based tandem solar cells, which are appearing as a next avenue of research to harness the solar energy more effectively. Recent experiments and theoretical studies revealed that CIGS in combination with another similar type absorbers (like CGS/CIS) or with other efficient absorbers (*e.g.* perovskite and Si-based) could boost the *PCE* considerably under different device architectures (like monolithic or 2/4-terminal) owing to different optical bandgaps of them, which absorb more amount of photons from a wider solar spectrum (Mufti et al., 2020; Powalla et al., 2018; Shen et al., 2018). However, there is a lack of exploration, where ALD-grown buffer layers have been used in such investigations. Therefore, further research

on the existing ALD-grown buffer layers, addressing the above issues, is supposed to accelerate the acceptability of ALD toward commercial production of CIGS TFSCs.

5. Conclusion

This review article presents a systematic and detailed study on ALD-grown buffer layers adopted so far in CIGS-based TFSCs. It clearly established the success of ALD in growing alternate buffer layers that can potentially replace the conventional CdS buffer layer. The article further discussed the search for a buffer layer with optimum CBO that eventually resulted in developing several Zn-based ternary buffer layers by ALD. Zn(O,S), ZnMgO, and ZnSnO among others, were found to be the most efficient buffer layers that yielded the highest *PCEs* for CIGS TFSCs till date. It could be concluded that the ALD has the highest potential towards optimizing the layer thickness and the ratio of the different elements in these ternary buffer layers. In addition, ALD was successfully adopted to grow other potential buffer layers (*e.g.* In_2S_3). Considering that there seems some stagnancy presently in the *PCE* of CIGS TFSCs, various remedial measures to overcome this situation are identified and discussed for their successful contribution into the field of solar PV in the future.

Declaration of Competing Interest

The authors declare that they have no known competing financial interests or personal relationships that could have appeared to influence the work reported in this paper.

Acknowledgment

This work was supported by the National Research Foundation of Korea (NRF) grant funded by the Korea government (2018R1A2B6002268 and 2019M1A2A2072421). This work was also supported by the Ministry of Trade, Industry & Energy (#10080651) and KSRC (Korea Semiconductor Research Consortium) support program for the development of the future semiconductor device.

References

Abou-Ras, D., Rudmann, D., Kostorz, G., Spiering, S., Powalla, M., Tiwari, A., 2005. Microstructural and chemical studies of interfaces between Cu(In,Ga)Se_2 and In_2S_3 layers. J. Appl. Phys. 97 (8), 084908.

Agbenyeke, R.E., Song, S., Park, B.K., Kim, G.H., Yun, J.H., Chung, T.-M., Kim, C.G., Han, J.H., 2018. Band gap engineering of atomic layer deposited $Zn_xSn_{1-x}O$ buffer for efficient Cu(In, Ga)Se_2 solar cell. Prog. Photovolt: Res. Appl. 26 (9), 745–751.

Asaduzzaman, M., Hasan, M., Bahar, A.N., 2016. An investigation into the effects of band gap and doping concentration on Cu(In,Ga)Se_2 solar cell efficiency. SpringerPlus 5 (1), 578.

Bakke, J.R., Pickrahn, K.L., Brennan, T.P., Bent, S.F., 2011. Nanoengineering and interfacial engineering of photovoltaics by atomic layer deposition. Nanoscale 3 (9), 3482–3508.

Baosheng, S., Akira, Y., Makoto, K., 1998. Textured ZnO thin films for solar cells grown by a two-step process with the atomic layer deposition technique. Jpn. J. Appl. Phys. 37 (2B), L206.

Baosheng, S., Koji, D., Akira, Y., Makoto, K., 1999. High-efficiency amorphous silicon solar cells with ZnO as front contact. Jpn. J. Appl. Phys. 38 (9R), 4983.

Bauhuis, G.J., Mulder, P., Haverkamp, E.J., Huijben, J.C.C.M., Schermer, J.J., 2009. 26.1% thin-film GaAs solar cell using epitaxial lift-off. Sol. Energy Mater. Sol. Cells 93 (9), 1488–1491.

Bin Mo, C., Park, S.J., Bae, S., Lim, M.-H., Nam, J., Kim, D., Yang, J., Suh, D., Min, B.K., Kim, D., Kang, Y., Kim, Y.-S., Lee, H.-S., 2019. Impact of buffer layer process and Na on shunt paths of monolithic series-connected CIGSSe Thin film solar cells. Sci. Rep. 9 (1), 3666.

Bissig, B., Carron, R., Greuter, L., Nishiwaki, S., Avancini, E., Andres, C., Feurer, T., Buecheler, S., Tiwari, A.N., 2018. Novel back contact reflector for high efficiency and double-graded Cu(In,Ga)Se_2 thin-film solar cells. Prog. Photovolt. Res. Appl. 26 (11), 894–900.

Bugot, C., Bouttemy, M., Schneider, N., Etcheberry, A., Lincot, D., Donsanti, F., 2018. New insights on the chemistry of plasma-enhanced atomic layer deposition of indium oxysulfide thin films and their use as buffer layers in Cu(In,Ga)Se_2 thin film solar cell. J. Vac. Sci. Technol. A 36 (6), 061510.

Burke, M., Blake, A., Djara, V., O'Connell, D., Povey, I.M., Cherkaoui, K., Monaghan, S., Scully, J., Murphy, R., Hurley, P.K., Pemble, M.E., Quinn, A.J., 2015. High aspect ratio iridescent three-dimensional metal–insulator–metal capacitors using atomic layer deposition. J. Vac. Sci. Technol. A 33 (1), 01A103.

Campbell, S., Qu, Y., Gibbon, J., Edwards, H.J., Dhanak, V.R., Tiwari, D., Barrioz, V., Beattie, N.S., Zoppi, G., 2020. Defect limitations in $Cu_2ZnSn(S, Se)_4$ solar cells utilizing an In_2S_3 buffer layer. J. Appl. Phys. 127 (20), 205305.

Chaisitsak, S., Sugiyama, T., Yamada, A., Konagai, M., 1999. Cu(InGa)Se_2 thin-film solar cells with high resistivity ZnO buffer layers deposited by atomic layer deposition. Jpn. J. Appl. Phys. 38 (9R), 4989.

Chaisitsak, S., Yamada, A., Konagai, M., Saito, K., 2000. Improvement in performances of ZnO:B/i-ZnO/Cu(InGa)Se_2 solar cells by surface treatments for Cu(InGa)Se_2. Jpn. J. Appl. Phys. 39 (4R), 1660.

Chantana, J., Kawano, Y., Nishimura, T., Kato, T., Sugimoto, H., Minemoto, T., 2019. Characteristics of $Zn_{1-x}Mg_xO$:B and its application as transparent conductive oxide layer in Cu(In,Ga)(S,Se)$_2$ solar cells with and without CdS buffer layer. Sol. Energy 184, 553–560.

Chantana, J., Kawano, Y., Nishimura, T., Kimoto, Y., Kato, T., Sugimoto, H., Minemoto, T., 2020a. 22%-efficient Cd-free Cu(In,Ga)(S,Se)$_2$ solar cell by all-dry process using $Zn_{0.8}Mg_{0.2}O$ and $Zn_{0.9}Mg_{0.1}O$:B as buffer and transparent conductive oxide layers. Prog. Photovolt: Res. Appl. 28 (1), 79–89.

Chantana, J., Kawano, Y., Nishimura, T., Kimoto, Y., Kato, T., Sugimoto, H., Minemoto, T., 2020b. Transparent electrode and buffer layer combination for reducing carrier recombination and optical loss realizing over a 22%-efficient Cd-free alkaline-treated Cu(In,Ga)(S,Se)$_2$ solar cell by the all-dry process. ACS Appl. Mater. Interfaces 12 (19), 22298–22307.

Chirilă, A., Buecheler, S., Pianezzi, F., Bloesch, P., Gretener, C., Uhl, A.R., Fella, C., Kranz, L., Perrenoud, J., Seyrling, S., Verma, R., Nishiwaki, S., Romanyuk, Y.E., Bilger, G., Tiwari, A.N., 2011. Highly efficient Cu(In,Ga)Se_2 solar cells grown on flexible polymer films. Nat. Mater. 10, 857.

Chirilă, A., Reinhard, P., Pianezzi, F., Bloesch, P., Uhl, A.R., Fella, C., Kranz, L., Keller, D., Gretener, C., Hagendorfer, H., Jaeger, D., Erni, R., Nishiwaki, S., Buecheler, S., Tiwari, A.N., 2013. Potassium-induced surface modification of Cu(In,Ga)Se_2 thin films for high-efficiency solar cells. Nat. Mater. 12, 1107.

CIGS-PV, 2015. White paper for cigs thin film solar cell technology (accessed: 17/10/2019). Available from: https://cigs-pv.net/wortpresse/wp-content/uploads/2015/12/CIGS-WhitePaper.pdf.

CIGS-PV, 2019. CIGS white paper (accessed: 17/10/2019). Available from: https://cigspv.net/wortpresse/wp-content/uploads/2019/04/CIGS_White_Paper_2019_online.pdf.

Contreras, M.A., Tuttle, J., Gabor, A., Tennant, A., Ramanathan, K., Asher, S., Franz, A., Keane, J., Wang, L., Scofield, J., Noufi, R., 1994. High efficiency Cu(In,Ga)Se_2-based solar cells: processing of novel absorber structures. In: Proceedings of 1994 IEEE 1st World Conference on Photovoltaic Energy Conversion - WCPEC (A Joint Conference of PVSC, PVSEC and PSEC), 61, pp. 68–75.

Delft, J.A.V., Garcia-Alonso, D., Kessels, W.M.M., 2012. Atomic layer deposition for photovoltaics: applications and prospects for solar cell manufacturing. Semicond. Sci. Technol. 27(7), 074002.

Dhara, A., Saha, D., Mitra, S., Sarkar, S.K., 2020. Atomic layer deposition of nitrogen incorporated molybdenum oxide: Unveiling carrier transport mechanism and its application in Li-ion battery. J. Vac. Sci. Technol. A 38 (2), 022409.

Eisgruber, I.L., Granata, J.E., Sites, J.R., Hou, J., Kessler, J., 1998. Blue-photon modification of nonstandard diode barrier in $CuInSe_2$ solar cells. Sol. Energy Mater. Sol. Cells 53 (3), 367–377.

Eldallal, G.M., Abou-Elwafa, M.S., Elgammal, M.A., Bedair, S.M., 1995. $Al_{0.3}Ga_{0.7}As$/GaAs concentrator solar cells. Renew. Energy 6 (7), 713–718.

Farhadi, B., Naseri, M., 2016. An optimized efficient dual junction InGaN/CIGS solar cell: A numerical simulation. Superlattices Microstruct. 96, 104–110.

Feurer, T., Reinhard, P., Avancini, E., Bissig, B., Löckinger, J., Fuchs, P., Carron, R., Weiss, T.P., Perrenoud, J., Stutterheim, S., Buecheler, S., Tiwari, A.N., 2017. Progress in thin film CIGS photovoltaics – Research and development, manufacturing, and applications. Prog. Photovolt: Res. Appl. 25 (7), 645–667.

Furlong, M.J., Froment, M., Bernard, M.C., Cortès, R., Tiwari, A.N., Krejci, M., Zogg, H., Lincot, D., 1998. Aqueous solution epitaxy of CdS layers on $CuInSe_2$. J. Cryst. Growth 193 (1), 114–122.

Genevée, P., Darga, A., Longeaud, C., Lincot, D., Donsanti, F., 2015. Atomic layer deposition of $ZnIn_xS_y$ buffer layers for Cu(In,Ga)Se_2 solar cells. J. Renewable Sustainable Energy 7 (1), 013116.

Genevée, P., Donsanti, F., Renou, G., Lincot, D., 2011. Study of growth mechanism and properties of zinc indium sulfide thin films deposited by atomic layer chemical vapor deposition over the entire range of composition. J. Phys. Chem. C 115 (34), 17197–17205.

Genevée, P., Donsanti, F., Schneider, N., Lincot, D., 2013. Atomic layer deposition of zinc indium sulfide films: Mechanistic studies and evidence of surface exchange reactions and diffusion processes. J. Vac. Sci. Technol. A 31 (1), 01A131.

Green, M.A., Emery, K., Hishikawa, Y., Warta, W., Dunlop, E.D., Levi, D.H., Ho-Baillie, A.W.Y., 2017. Solar cell efficiency tables (version 49). Prog. Photovolt: Res. Appl. 25 (1), 3–13.

Green, M.A., Hishikawa, Y., Dunlop, E.D., Levi, D.H., Hohl-Ebinger, J., Ho-Baillie, A.W.Y., 2018. Solar cell efficiency tables (version 52). Prog. Photovolt: Res. Appl. 26 (7), 427–436.

Guan, C., Wang, J., 2016. Recent development of advanced electrode materials by atomic layer deposition for electrochemical energy storage. Adv. Sci. 3 (10), 1500405.

Guillemoles, J.-F., Canava, B., Yousfi, E.B., Cowache, P., Galtayries, A., Asikainen, T., Powalla, M., Hariskos, D., Schock, H.-W., Lincot, D., 2001. Indium-based interface chemical engineering by electrochemistry and atomic layer deposition for copper indium diselenide solar cells. Jpn. J. Appl. Phys. 40 (10R), 6065.

Hakim, L.F., Blackson, J., George, S.M., Weimer, A.W., 2005. Nanocoating individual silica nanoparticles by atomic layer deposition in a fluidized bed reactor. Chem. Vap. Deposition 11 (10), 420–425.

Hayafuji, N., Eldallal, G.M., Dip, A., Colter, P.C., El-Masry, N.A., Bedair, S.M., 1994. Atomic layer epitaxy of device quality AlGaAs and AlAs. Appl. Surf. Sci. 82–83, 18–22.

Hegedus, S.S., Shafarman, W.N., 2004. Thin-film solar cells: device measurements and analysis. Prog. Photovolt: Res. Appl. 12 (2–3), 155–176.

Hong, H.K., Kim, I.Y., Shin, S.W., Song, G.Y., Cho, J.Y., Gang, M.G., Shin, J.C., Kim, J.H., Heo, J., 2016. Atomic layer deposited zinc oxysulfide n-type buffer layers for $Cu_2ZnSn(S,Se)_4$ thin film solar cells. Sol. Energy Mater. Sol. Cells 155, 43–50.

Hsu, W., Sutter-Fella, C.M., Hettick, M., Cheng, L., Chan, S., Chen, Y., Zeng, Y., Zheng, M., Wang, H.-P., Chiang, C.-C., Javey, A., 2015. Electron-selective TiO_2 contact for $Cu(In, Ga)Se_2$ solar cells. Sci. Rep. 5 (1), 16028.

Hultqvist, A., Edoff, M., Törndahl, T., 2011a. Evaluation of Zn-Sn-O buffer layers for $CuIn_{0.5}Ga_{0.5}Se_2$ solar cells. Prog. Photovolt: Res. Appl. 19 (4), 478–481.

Hultqvist, A., Platzer-Björkman, C., Coronel, E., Edoff, M., 2011b. Experimental investigation of $Cu(In_{1-x},Ga_x)Se_2/Zn(O_{1-z}, S_z)$ solar cell performance. Sol. Energy Mater. Sol. Cells 95 (2), 497–503.

Hultqvist, A., Platzer-Björkman, C., Pettersson, J., Törndahl, T., Edoff, M., 2009. $CuGaSe_2$ solar cells using atomic layer deposited Zn(O, S) and (Zn, Mg)O buffer layers. Thin Solid Films 517 (7), 2305–2308.

Hultqvist, A., Platzer-Björkman, C., Zimmermann, U., Edoff, M., Törndahl, T., 2012. Growth kinetics, properties, performance, and stability of atomic layer deposition Zn–Sn–O buffer layers for $Cu(In,Ga)Se_2$ solar cells. Prog. Photovolt: Res. Appl. 20 (7), 883–891.

Hwang, S., Larina, L., Lee, H., Kim, S., Choi, K.S., Jeon, C., Ahn, B.T., Shin, B., 2018. Wet pretreatment-induced modification of $Cu(In,Ga)Se_2$/Cd-free ZnTiO buffer interface. ACS Appl. Mater. Interfaces 10 (24), 20920–20928.

Illiberi, A., Frijters, C., Ruth, M., Bremaud, D., Poodt, P., Roozeboom, F., Bolt, P.J., 2018. Atmospheric spatial atomic layer deposition of ZnOS buffer layers for flexible $Cu(In, Ga)Se_2$ solar cells. J. Vac. Sci. Technol. A 36 (5), 051511.

Illiberi, A., Roozeboom, F., Poodt, P., 2012. Spatial atomic layer deposition of zinc oxide thin films. ACS Appl. Mater. Interfaces 4 (1), 268–272.

Ishizuka, S., Fons, P.J., 2020. Lithium-doping effects in $Cu(In,Ga)Se_2$ thin-film and photovoltaic properties. ACS Appl. Mater. Interfaces 12 (22), 25058–25065.

Jackson, P., Hariskos, D., Wuerz, R., Kiowski, O., Bauer, A., Friedlmeier, T.M., Powalla, M., 2015. Properties of $Cu(In,Ga)Se_2$ solar cells with new record efficiencies up to 21.7%. Phys. Status Solidi RRL 9 (1), 28–31.

Jackson, P., Wuerz, R., Hariskos, D., Lotter, E., Witte, W., Powalla, M., 2016. Effects of heavy alkali elements in $Cu(In,Ga)Se_2$ solar cells with efficiencies up to 22.6%. Phys. Status Solidi RRL 10 (8), 583–586.

Jayaraj, M.K., Saji, K.J., Nomura, K., Kamiya, T., Hosono, H., 2008. Optical and electrical properties of amorphous zinc tin oxide thin films examined for thin film transistor application. J. Vac. Sci. Technol., B: Microelectron. Process. Phenom. 26 (2), 495–501.

Kamada, R., Yagioka, T., Adachi, S., Handa, A., Tai, K.F., Kato, T., Sugimoto, H., 2016. New world record $Cu(In,Ga)(Se,S)_2$ thin film solar cell efficiency beyond 22%. In: 2016 IEEE 43rd Photovoltaic Specialists Conference (PVSC), pp. 1287–1291.

Kan, Z., Wang, Z., Firdaus, Y., Babics, M., Alshareef, Husam N., Beaujuge, P.M., 2018. Atomic-layer-deposited AZO outperforms ITO in high-efficiency polymer solar cells. J. Mater. Chem. A 6 (22), 10176–10183.

Kato, T., Wu, J., Hirai, Y., Sugimoto, H., Bermudez, V., 2019. Record Efficiency for Thin-Film Polycrystalline Solar Cells Up to 22.9% Achieved by Cs-Treated $Cu(In,Ga)(Se, S)_2$. IEEE J. Photovolt. 9 (1), 325–330.

Kaur, K., Kumar, N., Kumar, M., 2017. Strategic review of interface carrier recombination in earth abundant Cu–Zn–Sn–S–Se solar cells: current challenges and future prospects. J. Mater. Chem. A 5 (7), 3069–3090.

Kessler, F., Herrmann, D., Powalla, M., 2005. Approaches to flexible CIGS thin-film solar cells. Thin Solid Films 480–481, 491–498.

Khatri, I., Matsuyama, I., Yamaguchi, H., Fukai, H., Nakada, T., 2015. Surface sulfurization on MBE-grown $Cu(In_{1-x},Ga_x)Se_2$ thin films and devices. Jpn. J. Appl. Phys. 54 (8S1), 08KC10.

Kim, S., Mina, M.S., Kim, K., Gwak, J., Kim, J., 2020. Application of a Sn^{4+} doped In_2S_3 thin film in a CIGS solar cell as a buffer layer. Sustainable Energy Fuels 4 (1), 362–368.

Klenk, R., 2001. Characterisation and modelling of chalcopyrite solar cells. Thin Solid Films 387 (1), 135–140.

Ko, J.H., Kim, I.H., Kim, D., Lee, K.S., Lee, T.S., Cheong, B., Kim, W.M., 2007. Transparent and conducting Zn-Sn-O thin films prepared by combinatorial approach. Appl. Surf. Sci. 253 (18), 7398–7403.

Kobayashi, T., Jehl Li Kao, Z., Kato, T., Sugimoto, H., Nakada, T., 2016. A comparative study of Cd- and Zn-compound buffer layers on $Cu(In_{1-x},Ga_x)(S_y,Se_{1-y})_2$ thin film solar cells. Prog. Photovolt: Res. Appl. 24 (3), 389–396.

Kobayashi, T., Kumazawa, T., Kao, Z.J.L., Nakada, T., 2013. $Cu(In,Ga)Se_2$ thin film solar cells with a combined ALD-Zn(O, S) buffer and MOCVD-ZnO:B window layers. Sol. Energy Mater. Sol. Cells 119, 129–133.

Kodalle, T., Choubrac, L., Arzel, L., Schlatmann, R., Barreau, N., Kaufmann, C.A., 2019. Effects of KF and RbF post deposition treatments on the growth of the CdS buffer layer on CIGS thin films - a comparative study. Sol. Energy Mater. Sol. Cells 200, 109997.

Kong Fai, T., Rui, K., Takeshi, Y., Takuya, K., Hiroki, S., 2017. From 20.9 to 22.3% $Cu(In, Ga)(S,Se)_2$ solar cell: Reduced recombination rate at the heterojunction and the depletion region due to K-treatment. Jpn. J. Appl. Phys. 56 (8S2), 08MC03.

Kotipalli, R., Vermang, B., Joel, J., Rajkumar, R., Edoff, M., Flandre, D., 2015. Investigating the electronic properties of $Al_2O_3/Cu(In,Ga)Se_2$ interface. AIP Adv. 5 (10), 107101.

Larsson, F., Donzel-Gargand, O., Keller, J., Edoff, M., Törndahl, T., 2018. Atomic layer deposition of Zn(O, S) buffer layers for $Cu(In,Ga)Se_2$ solar cells with KF post-deposition treatment. Sol. Energy Mater. Sol. Cells 183, 8–15.

Larsson, F., Nilsson, N.S., Keller, J., Frisk, C., Kosyak, V., Edoff, M., Törndahl, T., 2017. Record 1.0 V open-circuit voltage in wide band gap chalcopyrite solar cells. Prog. Photovolt: Res. Appl. 25 (9), 755–763.

Le Tulzo, H., Schneider, N., Lincot, D., Donsanti, F., 2019. Toward an all-Atomic Layer Deposition (ALD) process for $Cu(In,Ga)(S,Se)_2$ (CIGS)-type solar cell. Sol. Energy Mater. Sol. Cells 200, 109965.

Lee, T.D., Ebong, A.U., 2017. A review of thin film solar cell technologies and challenges. Renewable Sustainable Energy Rev. 70, 1286–1297.

Li, D., Shi, J., Li, C., 2018. Transition-metal-based electrocatalysts as cocatalysts for photoelectrochemical water splitting: A mini review. Small 14 (23), 1704179.

Lindahl, J., Hägglund, C., Wätjen, J.T., Edoff, M., Törndahl, T., 2015. The effect of substrate temperature on atomic layer deposited zinc tin oxide. Thin Solid Films 586, 82–87.

Lindahl, J., Keller, J., Donzel-Gargand, O., Szaniawski, P., Edoff, M., Törndahl, T., 2016. Deposition temperature induced conduction band changes in zinc tin oxide buffer layers for $Cu(In,Ga)Se_2$ solar cells. Sol. Energy Mater. Sol. Cells 144, 684–690.

Lindahl, J., Wätjen, J.T., Hultqvist, A., Ericson, T., Edoff, M., Törndahl, T., 2013a. The effect of $Zn_{1-x}Sn_xO_y$ buffer layer thickness in 18.0% efficient Cd-free $Cu(In,Ga)Se_2$ solar cells. Prog. Photovolt: Res. Appl. 21 (8), 1588–1597.

Lindahl, J., Zimmermann, U., Szaniawski, P., Törndahl, T., Hultqvist, A., Salomé, P., Platzer-Björkman, C., Edoff, M., 2013b. Inline $Cu(In,Ga)Se_2$ Co-evaporation for high-efficiency solar cells and modules. IEEE J. Photovolt. 3 (3), 1100–1105.

Malm, U., Malmström, J., Platzer-Björkman, C., Stolt, L., 2005. Determination of dominant recombination paths in $Cu(In,Ga)Se_2$ thin-film solar cells with ALD–ZnO buffer layers. Thin Solid Films 480–481, 208–212.

Menner, R., Paetel, S., Wischmann, W., Powalla, M., 2017. Indium zinc oxide window layer for high-efficiency $Cu(In,Ga)Se_2$ solar cells. Thin Solid Films 634, 160–164.

Merdes, S., Malinen, V., Ziem, F., Lauermann, I., Schüle, M., Stober, F., Hergert, F., Papathanasiou, N., Schlatmann, R., 2014. Zn(O, S) buffer prepared by atomic layer deposition for sequentially grown $Cu(In,Ga)(Se,S)_2$ solar cells and modules. Sol. Energy Mater. Sol. Cells 126, 120–124.

Merdes, S., Ziem, F., Lavrenko, T., Walter, T., Lauermann, I., Klingsporn, M., Schmidt, S., Hergert, F., Schlatmann, R., 2015. Above 16% efficient sequentially grown $Cu(In,Ga)(Se,S)_2$-based solar cells with atomic layer deposited Zn(O, S) buffers. Prog. Photovolt: Res. Appl. 23 (11), 1493–1500.

Minemoto, T., Matsui, T., Takakura, H., Hamakawa, Y., Negami, T., Hashimoto, Y., Uenoyama, T., Kitagawa, M., 2001. Theoretical analysis of the effect of conduction band offset of window/CIS layers on performance of CIS solar cells using device simulation. Sol. Energy Mater. Sol. Cells 67 (1), 83–88.

Moriga, T., Hayashi, Y., Kondo, K., Nishimura, Y., Murai, K.-I., Nakabayashi, I., Fukumoto, H., Tominaga, K., 2004. Transparent conducting amorphous Zn–Sn–O films deposited by simultaneous dc sputtering. J. Vac. Sci. Technol. A 22 (4), 1705–1710.

Mufti, N., Amrillah, T., Taufiq, A., Sunaryono, Aripriharta, Diantoro, M., Zulhadjri, Nur, H., 2020. Review of CIGS-based solar cells manufacturing by structural engineering. Sol. Energy 207, 1146–1157.

Mughal, M.A., Engelken, R., Sharma, R., 2015. Progress in indium (III) sulfide (In_2S_3) buffer layer deposition techniques for CIS, CIGS, and CdTe-based thin film solar cells. Sol. Energy 120, 131–146.

Nadenau, V., Rau, U., Jasenek, A., Schock, H.W., 2000. Electronic properties of $CuGaSe_2$-based heterojunction solar cells. Part I. Transport analysis. J. Appl. Phys. 87 (1), 584–593.

Naghavi, N., Abou-Ras, D., Allsop, N., Barreau, N., Bücheler, S., Ennaoui, A., Fischer, C.-H., Guillen, C., Hariskos, D., Herrero, J., Klenk, R., Kushiya, K., Lincot, D., Menner, R., Nakada, T., Platzer-Björkman, C., Spiering, S., Tiwari, A.N., Törndahl, T., 2010. Buffer layers and transparent conducting oxides for chalcopyrite $Cu(In,Ga)(S,Se)_2$ based thin film photovoltaics: present status and current developments. Prog. Photovolt: Res. Appl. 18 (6), 411–433.

Naghavi, N., Spiering, S., Powalla, M., Cavana, B., Lincot, D., 2003. High-efficiency copper indium gallium diselenide (CIGS) solar cells with indium sulfide buffer layers deposited by atomic layer chemical vapor deposition (ALCVD). Prog. Photovolt: Res. Appl. 11 (7), 437–443.

Nakamura, M., Yamaguchi, K., Kimoto, Y., Yasaki, Y., Kato, T., Sugimoto, H., 2019. Cd-Free $Cu(In, Ga)(Se,S)_2$ Thin-Film Solar Cell With Record Efficiency of 23.35%. IEEE J. Photovolt. 9 (6), 1863–1867.

Nakashima, K., Kumazawa, T., Kobayashi, T., Mise, T., Nakada, T., 2012. Wide-Gap $Cu(In,Ga)Se_2$ solar cells with Zn(O, S) buffer layers prepared by atomic layer deposition. Jpn. J. Appl. Phys. 51, 10NC15.

Nandi, D.K., Sahoo, S., Kim, T.H., Cheon, T., Sinha, S., Rahul, R., Jang, Y., Bae, J.-S., Heo, J., Shim, J.-J., Kim, S.-H., 2018. Low temperature atomic layer deposited molybdenum nitride-Ni-foam composite: An electrode for efficient charge storage. Electrochem. Commun. 93, 114–118.

O'Neill, B.J., Jackson, D.H.K., Lee, J., Canlas, C., Stair, P.C., Marshall, C.L., Elam, J.W., Kuech, T.F., Dumesic, J.A., Huber, G.W., 2015. Catalyst design with atomic layer deposition. ACS Catal. 5 (3), 1804–1825.

Nandi, D.K., Yeo, S., Ansari, M.Z., Sinha, S., Cheon, T., Kwon, J., Kim, H., Heo, J., Song, T., Kim, S.-H., 2019. Thickness-dependent electrochemical response of plasma enhanced atomic layer deposited WS_2 anodes in Na-ion battery. Electrochim. Acta 322, 134766.

Ochoa, M., Buecheler, S., Tiwari, A.N., Carron, R., 2020. Challenges and opportunities for an efficiency boost of next generation Cu(In,Ga)Se_2 solar cells: prospects for a paradigm shift. Energy Environ. Sci. 13 (7), 2047–2055.
Ohtake, Y., Kushiya, K., Ichikawa, M., Yamada, A., Konagai, M., 1995. Polycrystalline Cu(InGa)Se_2 thin-film solar cells with ZnSe buffer layers. Jpn. J. Appl. Phys. 34 (11R), 5949.
Olsen, L.C., Aguilar, H., Addis, F.W., Wenhua, L., Jun, L., 1996. CIS solar cells with ZnO buffer layers. In: Conference Record of the Twenty Fifth IEEE Photovoltaic Specialists Conference - 1996, pp. 997–1000.
Otte, K., Makhova, L., Braun, A., Konovalov, I., 2006. Flexible Cu(In,Ga)Se_2 thin-film solar cells for space application. Thin Solid Films 511–512, 613–622.
Park, J., Huang, J., Yun, J., Liu, F., Ouyang, Z., Sun, H., Yan, C., Sun, K., Kim, K., Seidel, J., Chen, S., Green, M.A., Hao, X., 2018. The role of hydrogen from ALD-Al_2O_3 in kesterite Cu_2ZnSnS_4 solar cells: grain surface passivation. Adv. Energy Mater. 8 (23), 1701940.
Peng, C.-Y., Dhakal, T.P., Garner, S., Cimo, P., Lu, S., Westgate, C.R., 2014. Fabrication of Cu_2ZnSnS_4 solar cell on a flexible glass substrate. Thin Solid Films 562, 574–577.
Perkins, J.D., del Cueto, J.A., Alleman, J.L., Warmsingh, C., Keyes, B.M., Gedvilas, L.M., Parilla, P.A., To, B., Readey, D.W., Ginley, D.S., 2002. Combinatorial studies of Zn-Al-O and Zn-Sn-O transparent conducting oxide thin films. Thin Solid Films 411 (1), 152–160.
Pettersson, J., Platzer-Björkman, C., Edoff, M., 2009. Temperature-dependent current-voltage and lightsoaking measurements on Cu(In,Ga)Se_2 solar cells with ALD-$Zn_{1-x}Mg_xO$ buffer layers. Prog. Photovolt: Res. Appl. 17 (7), 460–469.
Pettersson, J., Törndahl, T., Platzer-Björkman, C., Hultqvist, A., Edoff, M., 2013. The influence of absorber thickness on Cu(In,Ga)Se_2 solar cells with different buffer layers. IEEE J. Photovolt. 3 (4), 1376–1382.
Platzer-Björkman, C., Barreau, N., Bär, M., Choubrac, L., Grenet, L., Heo, J., Kubart, T., Mittiga, A., Sanchez, Y., Scragg, J., Sinha, S., Valentini, M., 2019. Back and front contacts in kesterite solar cells: state-of-the-art and open questions. J. Phys. Energy 1 (4), 044005.
Platzer-Björkman, C., Kessler, J., Stolt, L., 2003a. Analysis of Zn(O, S) films for Cu(In,Ga)Se_2 solar cells. In: Proceedings-Estonian Academy Of Sciences Physics Mathematics, vol. 1999. Estonian Academy Publishers, pp. 299–307.
Platzer-Björkman, C., Kessler, J., Stolt, L., 2003b. Atomic layer deposition of Zn(O, S) buffer layers for high efficiency Cu(In,Ga)Se_2 solar cells. In: Proceedings of 3rd World Conference on Photovoltaic Energy Conversion, 2003. IEEE, pp. 461–464.
Platzer-Björkman, C., Lu, J., Kessler, J., Stolt, L., 2003c. Interface study of $CuInSe_2$/ZnO and Cu(In,Ga)Se_2/ZnO devices using ALD ZnO buffer layers. Thin Solid Films 431, 321–325.
Platzer-Björkman, C., Törndahl, T., Abou-Ras, D., Malmström, J., Kessler, J., Stolt, L., 2006. Zn(O, S) buffer layers by atomic layer deposition in Cu(In,Ga)Se_2 based thin film solar cells: band alignment and sulfur gradient. J. Appl. Phys. 100 (4), 044506.
Platzer-Björkman, C., Törndahl, T., Hultqvist, A., Kessler, J., Edoff, M., 2007. Optimization of ALD-(Zn, Mg)O buffer layers and (Zn, Mg)O/Cu(In,Ga)Se_2 interfaces for thin film solar cells. Thin Solid Films 515 (15), 6024–6027.
Powalla, M., Paetel, S., Ahlswede, E., Wuerz, R., Wessendorf, C.D., Friedlmeier, T.M., 2018. Thin-film solar cells exceeding 22% solar cell efficiency: An overview on CdTe-, Cu(In,Ga)Se_2-, and perovskite-based materials. Appl. Phys. Rev. 5 (4), 041602.
Pudov, A.O., Kanevce, A., Al-Thani, H.A., Sites, J.R., Hasoon, F.S., 2005. Secondary barriers in CdS–$CuIn_{1-x}Ga_xSe_2$ solar cells. J. Appl. Phys. 97 (6), 064901.
Ramanujam, J., Singh, U.P., 2017. Copper indium gallium selenide based solar cells – a review. Energy Environ. Sci. 10 (6), 1306–1319.
Ramesh, R., Sawant, S.Y., Nandi, D.K., Kim, T.H., Kim, D.H., Han, S.-M., Jang, Y., Ha, M. G., Cho, M.H., Yoon, T., Kim, S.-H., 2020. Hydrogen evolution reaction by atomic layer-deposited monx on porous carbon substrates: the effects of porosity and annealing on catalyst activity and stability. ChemSusChem 13 (16), 4159–4168.
Rau, U., Braunger, D., Herberholz, R., Schock, H.W., Guillemoles, J.-F., Kronik, L., Cahen, D., 1999. Oxygenation and air-annealing effects on the electronic properties of Cu(In,Ga)Se_2 films and devices. J. Appl. Phys. 86 (1), 497–505.
Rau, U., Grabitz, P.O., Werner, J.H., 2004. Resistive limitations to spatially inhomogeneous electronic losses in solar cells. Appl. Phys. Lett. 85 (24), 6010–6012.
Rau, U., Schock, H.W., 1999. Electronic properties of Cu(In,Ga)Se_2 heterojunction solar cells–recent achievements, current understanding, and future challenges. Appl. Phys. A 69 (2), 131–147.
Reinhard, P., Bissig, B., Pianezzi, F., Hagendorfer, H., Sozzi, G., Menozzi, R., Gretener, C., Nishiwaki, S., Buecheler, S., Tiwari, A.N., 2015. Alkali-templated surface nanopatterning of chalcogenide thin films: A novel approach toward solar cells with enhanced efficiency. Nano Lett. 15 (5), 3334–3340.
Repins, I., Contreras, M.A., Egaas, B., DeHart, C., Scharf, J., Perkins, C.L., To, B., Noufi, R., 2008. 19·9%-efficient ZnO/CdS/CuInGaSe$_2$ solar cell with 81·2% fill factor. Prog. Photovolt: Res. Appl. 16 (3), 235–239.
Sáez-Araoz, R., Krammer, J., Harndt, S., Koehler, T., Krueger, M., Pistor, P., Jasenek, A., Hergert, F., Lux-Steiner, M.C., Fischer, C.-H., 2012. ILGAR In_2S_3 buffer layers for Cd-free Cu(In,Ga)(S,Se)$_2$ solar cells with certified efficiencies above 16%. Prog. Photovolt: Res. Appl. 20 (7), 855–861.
Salomé, P.M.P., Keller, J., Törndahl, T., Teixeira, J.P., Nicoara, N., Andrade, R.R., Stroppa, D.G., González, J.C., Edoff, M., Leitão, J.P., Sadewasser, S., 2017. CdS and $Zn_{1-x}Sn_xO_y$ buffer layers for CIGS solar cells. Sol. Energy Mater. Sol. Cells 159, 272–281.
Shah, A.V., Schade, H., Vanecek, M., Meier, J., Vallat-Sauvain, E., Wyrsch, N., Kroll, U., Droz, C., Bailat, J., 2004. Thin-film silicon solar cell technology. Prog. Photovolt: Res. Appl. 12 (2–3), 113–142.
Shen, H., Duong, T., Peng, J., Jacobs, D., Wu, N., Gong, J., Wu, Y., Karuturi, S.K., Fu, X., Weber, K., Xiao, X., White, T.P., Catchpole, K., 2018. Mechanically-stacked perovskite/CIGS tandem solar cells with efficiency of 23.9% and reduced oxygen sensitivity. Energy Environ. Sci. 11 (2), 394–406.
Shimizu, A., Chaisitsak, S., Sugiyama, T., Yamada, A., Konagai, M., 2000. Zinc-based buffer layer in the Cu(InGa)Se_2 thin film solar cells. Thin Solid Films 361, 193–197.
Siebentritt, S., 2004. Alternative buffers for chalcopyrite solar cells. Sol. Energy 77 (6), 767–775.
Sinha, S., Didwal, P.N., Nandi, D.K., Cho, J.Y., Kim, S.-H., Park, C.-J., Heo, J., 2019a. Atomic layer deposited-ZnO@3D-Ni-foam composite for Na-ion battery anode: A novel route for easy and efficient electrode preparation. Ceram. Int. 45 (1), 1084–1092.
Sinha, S., Didwal, P.N., Nandi, D.K., Verma, R., Cho, J.Y., Kim, S.-H., Park, C.-J., Heo, J., 2019b. Revealing the simultaneous effects of conductivity and amorphous nature of atomic-layer-deposited double-anion-based zinc oxysulfide as superior anodes in na-ion batteries. Small 15 (37), 1900595.
Sinha, S., Nandi, D.K., Kim, S.-H., Heo, J., 2018a. Atomic-layer-deposited buffer layers for thin film solar cells using earth-abundant absorber materials: A review. Sol. Energy Mater. Sol. Cells 176, 49–68.
Sinha, S., Ramasamy, H.V., Nandi, D.K., Didwal, P.N., Cho, J.Y., Park, C.-J., Lee, Y.-S., Kim, S.-H., Heo, J., 2018b. Atomic layer deposited zinc oxysulfide anodes in Li-ion batteries: an efficient solution for electrochemical instability and low conductivity. J. Mater. Chem. A 6 (34), 16515–16528.
Siol, S., Dhakal, T.P., Gudavalli, G.S., Rajbhandari, P.P., DeHart, C., Baranowski, L.L., Zakutayev, A., 2016. Combinatorial reactive sputtering of In_2S_3 as an alternative contact layer for thin film solar cells. ACS Appl. Mater. Interfaces 8 (22), 14004–14011.
Spiering, S., Eicke, A., Hariskos, D., Powalla, M., Naghavi, N., Lincot, D., 2004. Large-area Cd-free CIGS solar modules with In_2S_3 buffer layer deposited by ALCVD. Thin Solid Films 451, 562–566.
Spiering, S., Hariskos, D., Powalla, M., Naghavi, N., Lincot, D., 2003. CD-free Cu(In,Ga)Se_2 thin-film solar modules with In_2S_3 buffer layer by ALCVD. Thin Solid Films 431, 359–363.
Spiering, S., Hariskos, D., Schröder, S., Powalla, M., 2005. Stability behaviour of Cd-free Cu(In,Ga)Se_2 solar modules with In_2S_3 buffer layer prepared by atomic layer deposition. Thin Solid Films 480–481, 195–198.
Stamford, L., Azapagic, A., 2019. Environmental impacts of copper indium gallium-selenide (CIGS) photovoltaics and the elimination of cadmium through atomic layer deposition. Sci. Total Environ. 688, 1092–1101.
Sterner, J., Malmström, J., Stolt, L., 2005. Study on ALD In_2S_3/Cu(In,Ga)Se_2 interface formation. Prog. Photovolt: Res. Appl. 13 (3), 179–193.
Tadatsugu, M., Hideo, S., Shinzo, T., Hirotoshi, S., 1994. Highly transparent and conductive zinc-stannate thin films prepared by RF magnetron sputtering. Jpn. J. Appl. Phys. 33 (12A), L1693.
Takuya, K., 2017. Cu(In,Ga)(Se,S)$_2$ solar cell research in Solar Frontier: Progress and current status. Jpn. J. Appl. Phys. 56 (4S), 04CA02.
Tokio, N., Masayuki, M., 2002. 18% Efficiency Cd-Free Cu(In,Ga)Se_2 thin-film solar cells fabricated using chemical bath deposition (CBD)-ZnS buffer layers. Jpn. J. Appl. Phys. 41 (2B), L165.
Törndahl, T., Coronel, E., Hultqvist, A., Platzer-Björkman, C., Leifer, K., Edoff, M., 2009. The effect of $Zn_{1-x}Mg_xO$ buffer layer deposition temperature on Cu(In,Ga)Se_2 solar cells: A study of the buffer/absorber interface. Prog. Photovolt: Res. Appl. 17 (2), 115–125.
Törndahl, T., Platzer-Björkman, C., Kessler, J., Edoff, M., 2007. Atomic layer deposition of $Zn_{1-x}Mg_xO$ buffer layers for Cu(In,Ga)Se_2 solar cells. Prog. Photovolt: Res. Appl. 15 (3), 225–235.
Tran, M.H., Cho, J.Y., Sinha, S., Gang, M.G., Heo, J., 2018. Cu_2O/ZnO heterojunction thin-film solar cells: the effect of electrodeposition condition and thickness of Cu_2O. Thin Solid Films 661, 132–136.
Turcu, M., Pakma, O., Rau, U., 2002. Interdependence of absorber composition and recombination mechanism in Cu(In,Ga)(Se,S)$_2$ heterojunction solar cells. Appl. Phys. Lett. 80 (14), 2598–2600.
Vermang, B., Fjällström, V., Gao, X., Edoff, M., 2014. Improved rear surface passivation of Cu(In,Ga)Se_2 solar cells: A combination of an Al_2O_3 rear surface passivation layer and nanosized local rear point contacts. IEEE J. Photovolt. 4 (1), 486–492.
Vermang, B., Fjällström, V., Pettersson, J., Salomé, P., Edoff, M., 2013. Development of rear surface passivated Cu(In,Ga)Se_2 thin film solar cells with nano-sized local rear point contacts. Sol. Energy Mater. Sol. Cells 117, 505–511.
Wang, H., Cao, S., Yang, B., Li, H., Wang, M., Hu, X., Sun, K., Zang, Z., 2020. NH_4Cl-modified ZnO for High-Performance $CsPbIBr_2$ perovskite solar cells via low-temperature process. Sol. RRL 4 (1), 1900363.
Wang, L., Li, D.-B., Li, K., Chen, C., Deng, H.-X., Gao, L., Zhao, Y., Jiang, F., Li, L., Huang, F., He, Y., Song, H., Niu, G., Tang, J., 2017. Stable 6%-efficient Sb_2Se_3 solar cells with a ZnO buffer layer. Nat Energy 2 (4), 17046.
Wang, T., Luo, Z., Li, C., Gong, J., 2014. Controllable fabrication of nanostructured materials for photoelectrochemical water splitting via atomic layer deposition. Chem. Soc. Rev. 43 (22), 7469–7484.
Wang, W.-C., Tsai, M.-C., Yang, J., Hsu, C., Chen, M.-J., 2015. Efficiency enhancement of nanotextured black silicon solar cells using Al_2O_3/TiO_2 dual-layer passivation stack prepared by atomic layer deposition. ACS Appl. Mater. Interfaces 7 (19), 10228–10237.
Wen, X., He, Y., Chen, C., Liu, X., Yang, B., Leng, M., Song, H., Zeng, K., Li, D., Li, K., Gao, L., Tang, J., 2017. Magnetron sputtered ZnO buffer layer for Sb_2Se_3 thin film solar cells. Sol. Energy Mater. Sol. Cells 172, 74–81.
Wu, W., Cao, Y., Caspar, J.V., Guo, Q., Johnson, L.K., Mclean, R.S., Malajovich, I., Choudhury, K.R., 2014. Characterization of CZTSSe photovoltaic device with an atomic layer-deposited passivation layer. Appl. Phys. Lett. 105 (4), 042108.

Yang, B., Wang, M., Hu, X., Zhou, T., Zang, Z., 2019. Highly efficient semitransparent $CsPbIBr_2$ perovskite solar cells via low-temperature processed In_2S_3 as electron-transport-layer. Nano Energy 57, 718–727.
Yin, W.-J., Yang, J.-H., Kang, J., Yan, Y., Wei, S.-H., 2015. Halide perovskite materials for solar cells: a theoretical review. J. Mater. Chem. A 3 (17), 8926–8942.
Yoon, J.-H., Song, J., Lee, S.-J., 2011. Practical application of building integrated photovoltaic (BIPV) system using transparent amorphous silicon thin-film PV module. Sol. Energy 85 (5), 723–733.
Yoshiaki, H., Yasuyoshi, K., Akira, Y., 2014. Numerical study of $Cu(In,Ga)Se_2$ solar cell performance toward 23% conversion efficiency. Jpn. J. Appl. Phys. 53 (1), 012301.
Yoshiaki, H., Yukiya, H., Yasuyoshi, K., Akira, Y., 2012. Improvement of the band profile of $Cu(In,Ga)Se_2$ solar cells with high-Ga content prepared using a five-stage method. Jpn. J. Appl. Phys. 51 (10S), 10NC03.
Yousfi, E., Asikainen, T., Pietu, V., Cowache, P., Powalla, M., Lincot, D., 2000. Cadmium-free buffer layers deposited by atomic later epitaxy for copper indium diselenide solar cells. Thin Solid Films 361, 183–186.
Yousfi, E., Weinberger, B., Donsanti, F., Cowache, P., Lincot, D., 2001. Atomic layer deposition of zinc oxide and indium sulfide layers for $Cu(In,Ga)Se_2$ thin-film solar cells. Thin Solid Films 387 (1), 29–32.
Zang, Z., 2018. Efficiency enhancement of ZnO/Cu_2O solar cells with well oriented and micrometer grain sized Cu_2O films. Appl. Phys. Lett. 112 (4), 042106.